Tampere University

Jesper Leppinen

ADVANCED OPTICAL REFERENCING FOR WAVEGUIDE MEASUREMENT SYSTEM

Master of Science Thesis
Faculty of Engineering and Natural Sciences
Examiners: Assoc. Prof. Tapio Niemi
Dr. Thomas Kerst
August 2023

ABSTRACT

Jesper Leppinen: Advanced optical referencing for waveguide measurement system
Master of Science Thesis
Tampere University
Science and Engineering
August 2023

In the field of optical metrology, the impact of the measurement system must be considered on the measurements in order to prevent any unwanted influence on the measurement results and accurately quantify the devices under testing. This procedure is commonly referred to as referencing. However, referencing requires very careful matching of pupils within the measuring instrument, imposing some constraints on the optical design of optical metrology devices. As a consequence, it is frequently associated with high costs, slow manufacturing processes, and complexity. This thesis presents a method to remove the requirement for pupil matching, thereby potentially alleviating the challenges mentioned before.

This thesis is motivated by the current hardware limitation when measuring augmented reality waveguides. Most of the current waveguide designs require illuminating and imaging the waveguide on the same side. This causes a difficult challenge as the referencing requires the camera's and projector's pupils to be matched, instead of them being positioned next to each other. Currently, this pupil match is achieved by rotating the camera upside down so that the projector and camera are pointing at each other. This increases the cost and complexity of the system, decreases the Units Per Hour performance, and introduces inaccuracy.

In order to decrease the overall cost and complexity of the system, we have developed a method to do referencing without the need for a pupil match. The reason, why this hasn't been done earlier, is that the pupil mismatch introduces vignetting into the system and aberrations to the wavefront. In this thesis, we are going to show a method, called "field reconstruction", that overcomes these two problems and can reproduce the same information as the pupil-matched referencing.

In the first experiment, we test how much pupil mismatch and mirrors affect the modulation transfer function (MTF) values of near-diffraction-limited lenses. Basically, we validate the preservation of the wavefront at some field points with MTF measurements. In the second experiment, we show that the whole field can be reconstructed from vignetted images captured outside the pupil match. In addition, we will introduce two different algorithms to combine the vignetted images for this method.

Both of the measurements provide very promising results. These experiments prove that pupil matching is not mandatory as the full pupil can be scanned and combined to form the complete field. Fundamentally, this implies that the field reconstruction method can be used for referencing and consequently, remove the necessity for rotating the camera. This is a remarkable finding that will enable us to improve the current designs or create completely new measurement systems.

Keywords: pupil, field, image quality, MTF, referencing, waveguide, augmented reality

TIIVISTELMÄ

Jesper Leppinen: Optisen referenssimittauksen toteuttaminen aaltojohteiden mittausjärjestelmään
Diplomityö
Tampereen yliopisto
Teknis-luonnontieteellinen
Elokuu 2023

Optisten mittauslaitteiden oma vaikutus suoritettuihin mittauksiin on otettava huomioon, jotta voidaan välttää virheet mittaustuloksissa ja mahdollistaa mittauskohteiden tarkka kvantifiointi. Tämä vaikutus voidaan huomioida referenssimittauksella. Referenssimittaus kuitenkin vaatii erittäin huolellista pupillien kohdistusta, mikä asettaa rajoitteita optisten mittauslaitteiden suunnittelulle. Siitä seuraa yleensä haittapuolia, kuten korkeat kustannukset, hitaat valmistusprosessit ja monimutkaisuus. Tässä opinnäytetyössä esitellään menetelmä referenssimittaamiseen ilman pupillien kohdistamista lieventäen samalla edellä mainittuja haittoja.

Diplomityön taustalla on nykyisten laitteiden rajoitteet lisätyn todellisuuden aaltojohteita mitattaessa. Suurin osa nykyisistä aaltojohteista edellyttää niiden valaisemista ja kuvantamista samalta puolelta. Referenssimittaus vaatii kameran ja projektorin pupillien kohdistamisen, mikä toteutetaan kääntämällä kamera ylösalaisin referenssimittauksen ajaksi. Kameran kääntäminen edestakaisin referenssimittauksen vuoksi lisää sekä kustannuksia että monimutkaisuutta, hidastaa mittausprosessia ja lisää epätarkkuutta.

Tässä opinnäytetyössä esitellään menetelmä nimeltään "kenttärekonstruktio", jonka avulla voidaan suorittaa referenssimittaus ilman pupillien kohdistamista. Tämä vähentää sekä järjestelmän kokonaiskustannuksia että monimutkaisuutta. Perinteisesti referenssimittausta ilman pupillien kohdistamista ei tehdä, koska se normaalisti aiheuttaa optiseen systeemiin vinjetointia ja aaltorintamaan vääristymää. Kenttärekonstruktio-menetelmän avulla voidaan kuitenkin minimoida tai jopa välttää nämä ongelmat kokonaan sekä tuottaa sama informaatio kuin, jos pupillit olisivat kohdistettuina.

Ensimmäisessä kokeessa mitattiin lähes-diffraktiorajoitettujen linssien avulla, kuinka paljon pupillien kohdistamisen puute ja käytettävät peilit aiheuttavat eroja modulaationsiirtofunktioon. Käytännössä kyseisen mittauksen tarkoituksena on validoida aaltorintaman säilyminen tietyissä kohdissa kenttää käyttäen modulaationsiirtofunktiota. Toisessa kokeessa todistetaan, että koko kenttä voidaan rekonstruktoida kuvista, jotka ovat vinjetöityneitä pupillien epäkohdistuksen vuoksi. Lisäksi työssä esitetään kaksi erilaista algoritmia vinjetöityneiden kuvien yhdistämiseen.

Molemmat kokeet antavat erittäin lupaavia tuloksia. Nämä kokeet osoittavat, että pupillien kohdistaminen ei ole tarpeellista referenssimittauksen tekemiseen. Pohjimmiltaan tämä tarkoittaa sitä, että kenttärekonstruktio-menetelmää voidaan käyttää referenssimittauksen suorittamiseen ja sen seurauksena nykyinen kameran kääntäminen voidaan jättää pois. Tämä on merkittävä havainto, mikä mahdollistaa nykyisten mittauslaitteiden kehittämisen sekä uusien mittalaitteiden suunnittelun ja valmistamisen.

Avainsanat: pupilli, kenttä, kuvan laatu, MTF, referenssimittaus, aaltojohde, lisätty todellisuus

PREFACE

I am happy to present this thesis, the culmination of extensive research and experiments, conducted within the Optics Laboratory at OptoFidelity. This journey has been one of intellectual growth, innovative exploration, and collaborative effort, and I am profoundly grateful for the invaluable support and guidance I have received throughout this journey.

First and foremost, I want to express my gratitude to my co-workers at OptoFidelity. It has been a pleasure and honor to work with such talented colleagues. In addition, I want to give special thanks to my thesis supervisors, Dr. Thomas Kerst and Assoc. Prof. Tapio Niemi, who have been guiding and helping me during this thesis.

Personally, I want to thank my family and friends, who have been supporting and helping me during my student years. Their company has let me enjoy my time at the university and has given me better work-life balance. Needless to say, I have gained some unforgettable memories with them during these last six years.

In closing, I would like to express my deepest appreciation to everyone who played a role in making this thesis a reality. Your support, encouragement, and collaborative spirit have left an indelible mark on this work. As I present this thesis, I do so with the hope that this work will not only contribute to the continuous research in the field of optics but also serve as a source of inspiration for forthcoming innovations within this dynamic field.

Tampere, 31st August 2023

Jesper Leppinen

CONTENTS

LIST OF SYMBOLS AND ABBREVIATIONS

C	Contrast value
D	Dark frame image
F	Flat-field image
$F_{\max}$	Maximum pixel value of flat-field image
I_{corr}	Flat-field corrected image
L_{avg}	Average luminance value
L_{avg}	Maximum luminance value
M_{corr}	Flat-field correction matrix
PD	Distance between pupils
α	Field location angle
λ	Wavelength
CNU	Contrast non-uniformity
LNU	Luminance non-uniformity
ξ_{sensor}	resolution of the sensor
c	Speed of light in vacuum
f	Frequency
lp	Line pair
r_{Airy}	Airy disk radius
s	Pixel size
AC1	Autocollimator for tracking hexapod movement
AC2	Autocollimator for alignment experiment
ANSI	American National Standards Institute
AR	Augmented reality
DOF	Depth of field
DUT	Device under testing
ESF	Edge spread function
FFT	Fast Fourier transform

FOV	Field of view
IEC	International Electrotechnical Commission
ISO	International Organization for Standardization
LED	Light-emitting diode
LSF	Line spread function
MTF	Modulation transfer function
ND	Neutral density
OLED	Organic light-emitting diode
POC	Proof-of-concept
SID	Society for Information Display
TIR	Total internal reflection
VR	Virtual reality
WG-IQ	Waveguide image quality measurement system
XR	Extended reality

1. INTRODUCTION

In recent years, the augmented reality (AR) industry has begun to gain growth and popularity. However, the widespread adoption of AR technology in the consumer market is still hindered by various challenges, such as affordability, limited use cases, comfort, and social acceptance, among others. To achieve success in the consumer market, AR glasses must become not only affordable but also socially acceptable. Additionally, ensuring user comfort, optimal image quality, sufficient computing power, high-quality materials, and robust software functionalities are essential requirements that companies are continuously developing.

Leading technology companies, including Microsoft, Meta, Google, and recently Apple, have already unveiled their Extended Reality (XR) glasses. Simultaneously, numerous smaller companies such as Varjo, Lenovo, and Nreal are striving to gain a competitive edge in this fast-growing sector. As the demand for XR glasses increases, the need for mass production becomes necessary to enhance affordability and meet the demand. However, scaling up manufacturing requires substantial investments in automated production and quality control processes.

The optical waveguide plays a crucial role in determining the image quality of AR glasses, as it serves to guide the virtual image to the user's eye. Currently, there are four primary types of waveguide structures in use: reflective, polarized, diffractive, and holographic. However, the manufacturing process of waveguides is still in its developing phase and remains time-consuming, undergoing continuous development. As a consequence, the current measurement systems can be relatively complex, flexible, and slow. But it is expected that the main requirements are going to change once companies start to mass-produce waveguides

Image quality measurement systems contain two key components: the camera and the light engine. Several factors may impact the optical performance of the system over time, such as aging and wear-and-tear degradation. The system's performance is validated through referencing which traditionally has required a careful matching of the pupils. Because of the potential changes in optical performance, referencing has to be conducted periodically to maintain the system's accuracy and reliability. Consequently, robust and reliable referencing methods are essential to ensure the consistent and accurate assess-

ment of image quality for AR glasses.

In this thesis, a method for referencing without the need for pupil matching is presented. This method is called field reconstruction and it includes both imaging and image processing. This method is validated in two separate experiments which compare the pupil-matched reference image and the field-reconstructed reference image. This method can also be utilized in other applications that require pupil matching.

Chapter 2 presents the principles of optical imaging and describes basic optical phenomena. Chapter 3 introduces the basic waveguide structure and mainly focuses on the measurement of the image quality of the waveguide. The experimental parts of the thesis are presented in the Chapters 4 and 5. The first experiment includes investigating the effects of pupil mismatch on the MTF performance and the second experiment shows how the field reconstruction can be done with different algorithms. Lastly, the Chapter 6 presents a conclusion for this new referencing method.

2. PRINCIPLES OF OPTICAL IMAGING

Light is electromagnetic radiation, which can be described as coupled electric and magnetic fields propagating through space as a wave. [1] It has wave-particle duality which means that it can be thought of as both the particle and the wave at the same time. Light waves are characterized by their wavelength and frequency. The relationship between these two is

$$c = \lambda f, \tag{2.1}$$

where c is the speed of light in a vacuum, λ is wavelength and f is frequency. Electromagnetic radiation covers a large range of wavelengths, from gamma rays with wavelengths less than 10^{-11} meter up to radio waves with wavelengths measured in meters.

In the context of imaging optics, especially in augmented reality measurement applications, we are mostly interested in the visible range of the spectrum that covers only a small band of wavelengths, from about 380 to about 700 nm. The human eye can see the wavelength of 380 nm as violet and 700 nm as red. Inside this range, the human eye can perceive the different wavelengths as different colors. [2]

For the human eye to perceive light, it needs to interact with it somehow. The human vision is dependent on the fact that it can absorb light particles called photons. Humans can see objects because the photons reflect from the objects to our eyes. The eye then acts as a lens that bends the light to the back of our eyes, where it interacts with the retina, which converts the photons into electrical signals. Our brain then reacts to those electrical signals and forms an image that we can then see. The irradiance of light is directly proportional to the number of photons per unit area per unit time. [3] Cameras work similarly as they transform the energy from the photons to electrical charges and store the electrical signal captured by each pixel. Then the electrical signal can be processed and the image can be formed. [4]

2.1 Ray optics

Ray optics is also known as geometric optics or ray tracing. It provides a simplified description of light by ignoring the wave nature of light. The properties of light in ray optics

are governed by the laws of reflection and refraction. [1] These laws are well known and describe how the light rays interact with surfaces and boundaries between two different media. These properties are very useful in designing optical systems as they offer a method to determine the behavior of light rays between optical elements such as lenses and cameras and how they contribute to image formation.

The most important assumption in ray optics is that light rays travel in straight lines. We can use this assumption and the laws of reflection and refraction to form a method to determine the light's behavior. The law of reflection states that when a light ray hits a reflective surface, the angle of incidence is equal to the angle of reflection. This means that the incident ray, the normal of the surface, and the reflected ray are all in the same plane. This fundamental principle, shown in Fig. 2.1, describes the light's behavior when it interacts with mirrors and other reflective objects.

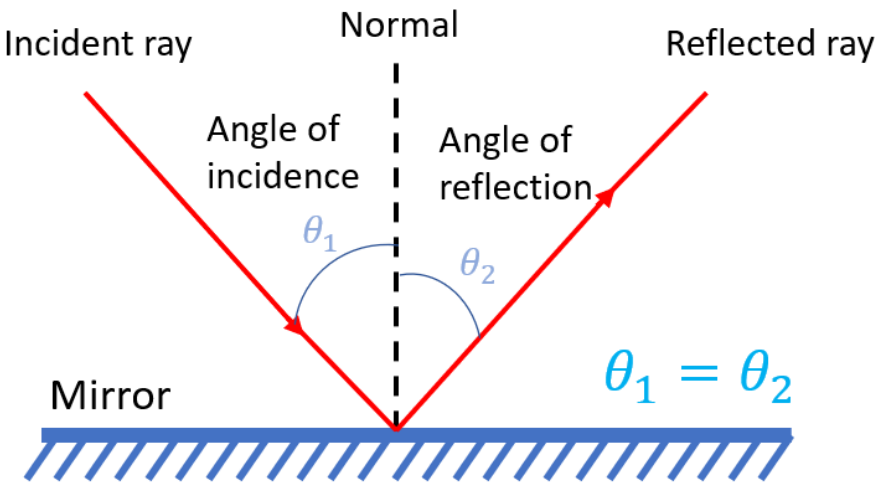

Figure 2.1. *Law of reflection*

The law of refraction, on the other hand, describes how light behaves when it goes from one medium to another. It can be derived from the wave behavior of light when the wavefront passes through the surface of the media. It is also known as Snell's law:

$$n_1 sin(\theta_1) = n_2 sin(\theta_2), \tag{2.2}$$

where n_1 is index of the first medium, θ_1 is the angle of incidence, n_2 is index of the second medium and θ_2 is the angle of refraction. According to Eq. 2.2, the light rays change direction and bend either towards or away from the normal, depending on the relative indices of refraction. This is shown in Fig. 2.2. Consequently, a critical angle can be derived from Snell's law. At the critical angle, the refracted ray makes an angle of 90 degrees with the normal. This critical angle, θ_c in Eq. 2.3, can be derived from Snell's law. [1] And at any higher angles of incidence, the ray will be totally reflected

inside the material. This is called total internal reflection (TIR) which is the foundation of waveguides.

$$sin(\theta_c) = \frac{n_2}{n_1} \tag{2.3}$$

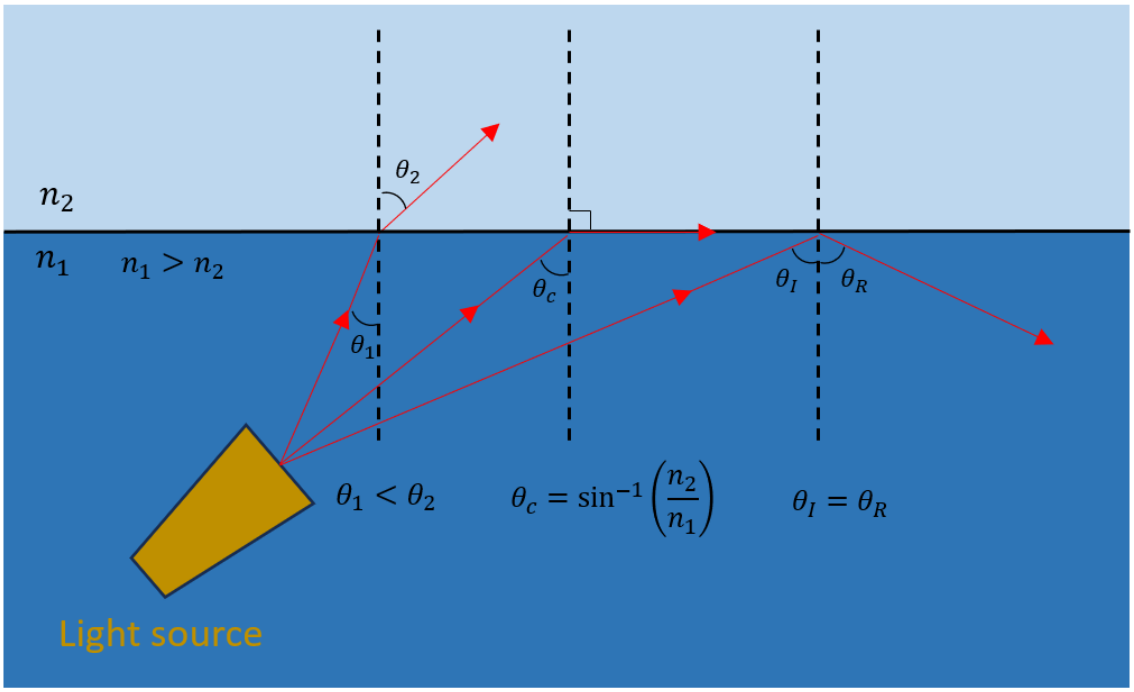

Figure 2.2. *Illustration of Snell's law, where* $n_1 > n_2$

These are fundamental principles of optics that allow us to predict and understand how light rays behave when they interact with lenses, prisms, or any other optical components.

Optical systems may contain different optical apertures that can limit the passage of light rays. However, some of the apertures are not relevant to the performance of the optical system. In order to make clear, what is relevant and what is not, the concepts of aperture stop, field stop, entrance pupil, and exit pupil have been formed. The aperture stop is the opening in the optical system that controls the amount of light entering the system. By adjusting the size of the aperture stop we can adjust the amount of light passing through to the camera sensor. [5] The aperture size will directly affect the used exposure time and the depth of field (DOF), which refers to the distance that is still in focus in the camera sensor. Field stop, on the other hand, defines the limit of the field of view (FOV) meaning that it limits the angular extent of the image that can be seen through the system. By reducing the field stop's size we can narrow down the FOV and thus see the center part of the image. [6] In addition, by reducing the aperture stop, optical designers can better control the aberrations, vignetting, and uniformity of the image. In illumination applications, such as in light engines, the field stop is used to narrow down the FOV of the projected beam. [7]

There are three primary rays that hold a particular interest in optics: the paraxial ray, the marginal ray, and the principle ray which is also known as a chief ray. These three different types of rays are illustrated in Fig. 2.3. The paraxial ray is a ray that has a very small angle with respect to the optical axis. If the angle of incidence of the ray on the refracting surface is small, the sine or tangent of any angle can be replaced with the angle itself. This is called paraxial approximation and it helps to simplify the calculations of the ray tracing. [8] The second one, the marginal ray, can be described as the ray that starts from the point where the object crosses the optical axis and touches the edge of the aperture stop of the system. It refers to the ray that passes through the outermost point of the object or scene being observed. [9] The marginal ray is especially informative while designing optical systems as it is directly related to the FOV. By analyzing marginal rays, optical designers can evaluate the image quality and aberrations on the edges of the image. The third one, the chief ray, is the ray that passes through the center of the aperture stop which acts as the entrance pupil. It is usually chosen as a reference ray because it has minimal deflection when passing through the optical system. By analyzing the chief ray the image height can be defined. [10, 11]

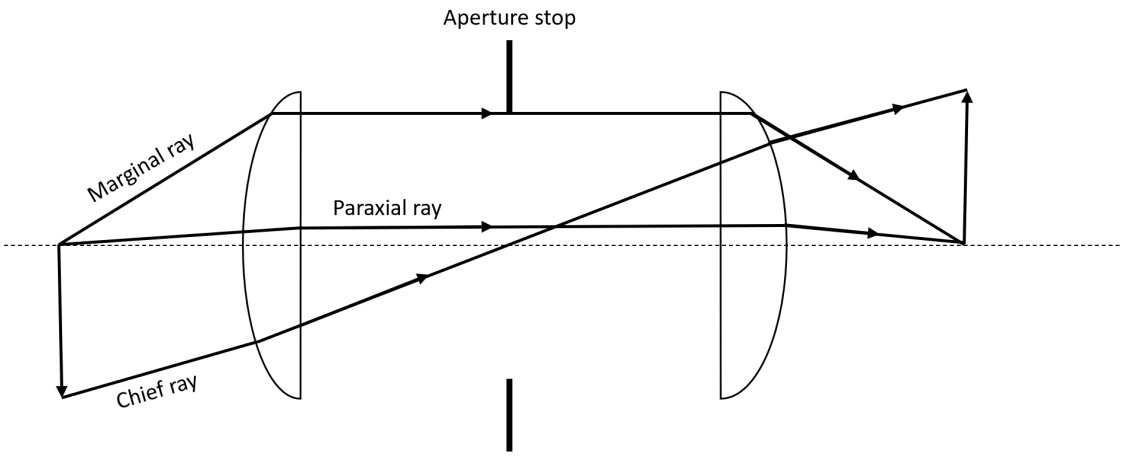

Figure 2.3. *Illustration of paraxial, chief and marignal rays.*

Essentially, ray tracing can be used to compute the exact trajectories of rays traveling through an optical system using the laws of reflection and refraction described above. In principle, ray optics is particularly useful if dealing with large-scale optical systems, where the wavelength is much smaller than the size of the objects and the scale of the system. It allows for straightforward optical simulations to be done. [5, 12]

Note that even though ray optics helps us design optical systems and make the simulations easier, it also has some negative effects. Ray optics neglects some of the important phenomena such as diffraction, interference, or polarization of light. All of these are also important to take into account when designing consumer applications such as AR or VR glasses.

2.2 Pupils and field

The concept of "field" is a multifaceted concept and holds significant importance in optics. It has different interpretations and implications in many different contexts. It can be used to represent the physical area or the angular range within the objects that can be seen through the system.

Although, in optics and imaging it is defined as the angular or spatial extent of the scene or object that can be captured or observed by a particular optical system or imaging device. It is often expressed as an angle or a physical dimension. The FOV in this context is related to parameters such as focal length, angular resolution, and sensor size. [13] On the other hand, in the context of VR, AR, and other computer graphics, the FOV is defined as the angular span of the virtual environment that is visible to the user. The FOV is important in AR applications, because the larger the FOV of the AR glasses, the more immersive they are. Therefore companies are developing and finding new ways to increase the FOV of their AR glasses. [14]

2.2.1 Entrance and exit pupils

Pupils are in general very important concepts in optics. There are two types of pupils in the optical system, entrance pupil and exit pupil. The entrance pupil is the opening of the lens seen from the object side. It limits the maximum angle of light rays that enters the optical system and thus affects the performance of the optical system. [7] The entrance pupil, illustrated in Fig. 2.4, is an important concept in optics because it directly influences the performance of the optical system.

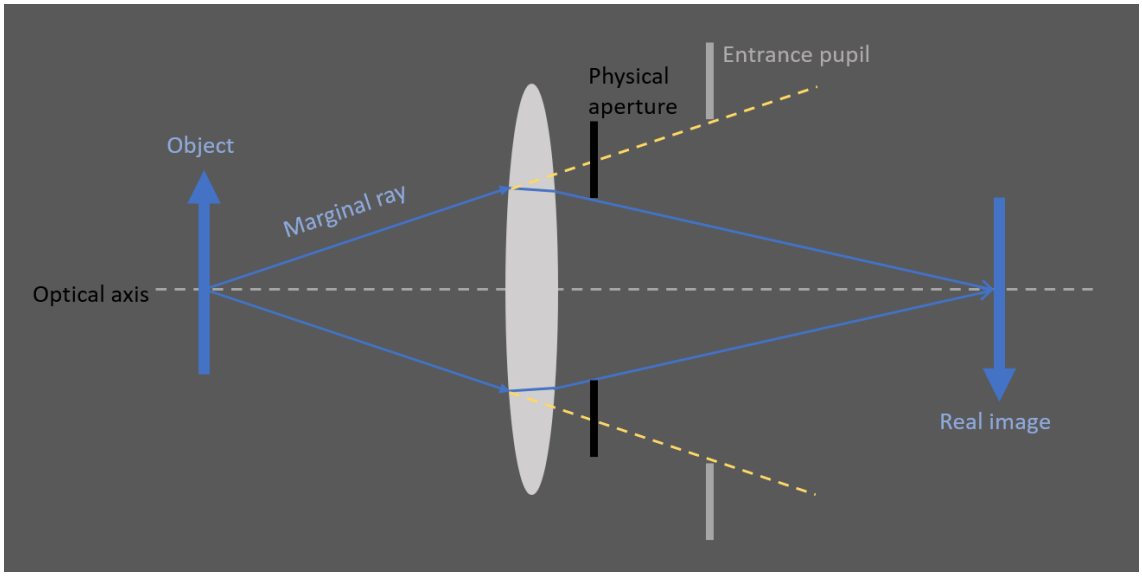

Figure 2.4. *The entrance pupil is the size of the physical aperture that would be required to pass the marginal ray if the lens were not present.*

The amount of light that can enter the system is directly proportional to the size of the entrance pupil. By increasing the size of the entrance pupil more light will go into the system. This would directly lead to a brighter image, which is crucial for example in low-light situations. Alternatively, optical designers can decrease the entrance pupil size to minimize stray light. Also, in photography, the DOF will be affected by the entrance pupil size. [15]

One example of the entrance pupil is the iris of the human eye. Humans adapt to different light conditions by adjusting the size of the iris by contracting and dilating it. This can be seen when the iris contracts in bright environments and dilates in low-light environments. The human eye can adjust the light entering the retina and protect the retina from excessive light by adjusting the size of the iris. [8]

In optics, the exit pupil is a virtual aperture in the optical system. Basically, it is the aperture seen from the image plane and can be described as the minimum diameter of light after leaving the optical system. [16] It limits the size of the light beam that reaches the observer's eye. It is illustrated in Fig. 2.5.

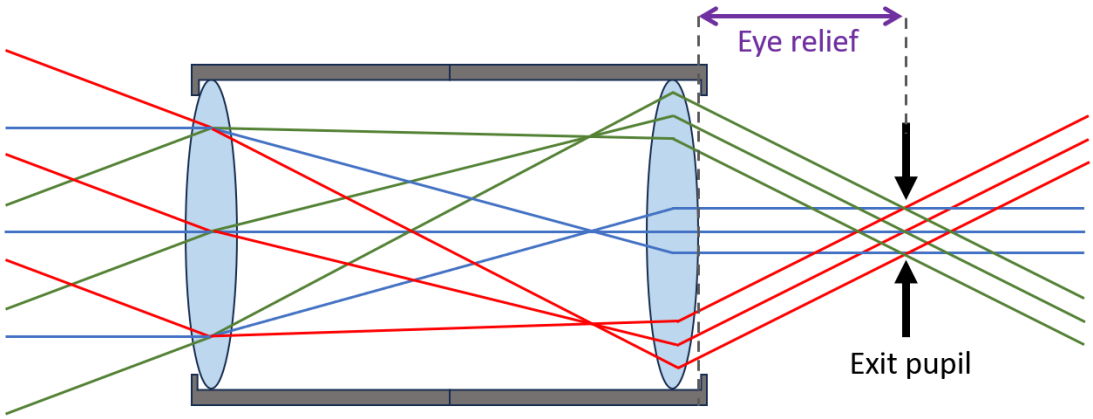

Figure 2.5. *Example of exit pupil.*

The exit pupil is a very important concept in applications, where we want to see the image through the optical system such as in telescopes or AR waveguides. [15] In order to maximize the properties of the optical instrument, the entrance pupil of the viewer's eye or lens must be aligned with and be similar in size to the instrument's exit pupil. This guarantees the coupling of the two optical systems and avoids vignetting. [8]

2.2.2 Pupil matching

Pupil matching refers to a situation where the exit pupil of an optical system is aligned to overlap with the entrance pupil of another optical system. It prevents any additional vignetting so that the entire FOV is visible. Usually, pupil matching causes limitations to the system and its performance. It can also be very difficult to achieve as it requires

precise alignments and accuracy of the optical systems. Even a small misalignment will cause vignetting that will decrease the performance of the system. [8] This misalignment is called pupil mismatch and it can happen both in the axial and lateral direction which is illustrated in Fig. 2.6.

Pupil matching in the axial direction requires the entrance pupil to be exactly in eye relief distance from the first optical system. Eye relief refers to the axial distance between the exit pupil and the last surface of the optical system. The user should be able to obtain the full FOV at eye relief distance. [16]

Pupil mismatch can also happen because of the lateral displacement of the pupils. If the exit pupil and the entrance pupil are exactly the same size, the alignment of the pupils must be perfect in order not to see vignetting. If the exit pupil is larger than the entrance pupil, it will naturally cause vignetting as some of the beams are lost outside the entrance pupil. In the case of a smaller exit pupil diameter, there would be more tolerance for pupil matching the two optical systems. This means that the full FOV would be still visible even if there was a small axial or lateral mismatch in eye relief as the exit pupil would still fit inside the entrance pupil. [17]

In the application of AR waveguides, a roughly 3 mm exit pupil and entrance pupil are desired as they mimic the average iris size of a human eye. In this case, the pupil match has to be perfect in order to perceive all the light without vignetting. [18] Even an infinitesimal mismatch in eye relief will cause light to be lost and thus the image to be vignetted. This happens due to the nature of the beam expansion after the exit pupil which can be seen in Fig. 2.5 as the distance between different field angles increases.

For accurate pupil matching, the pupil match can be ensured using the "knife-edge" method. It works by observing the image of a sharp edge and placing the knife edge near the exit pupil. Then the knife is moved across the exit pupil and thus blocks different parts of the exit pupil. The image is simultaneously monitored in case the image gets partially blocked or vignetted. If the image gets globally dimmer, the pupils are matched.

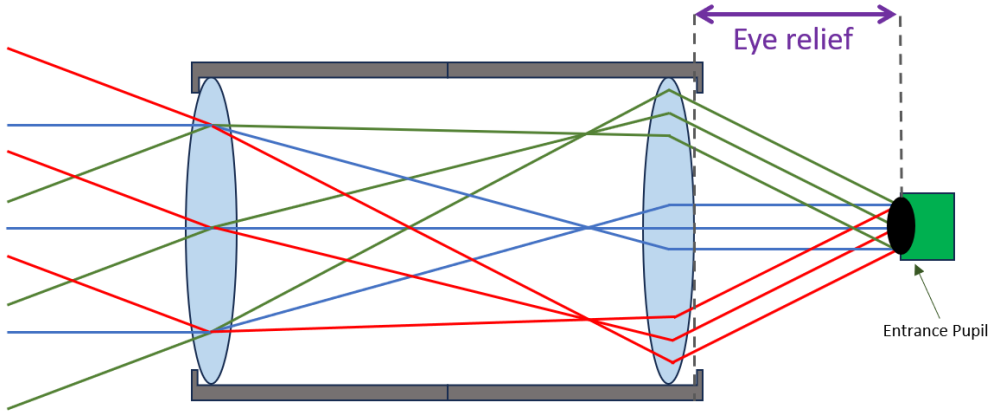

(a) *Pupil matched*

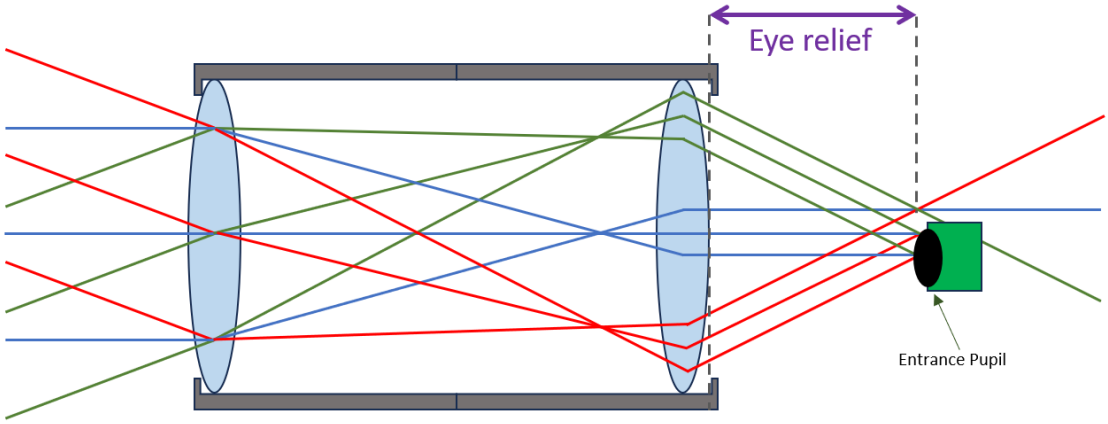

(b) *Lateral pupil mismatch*

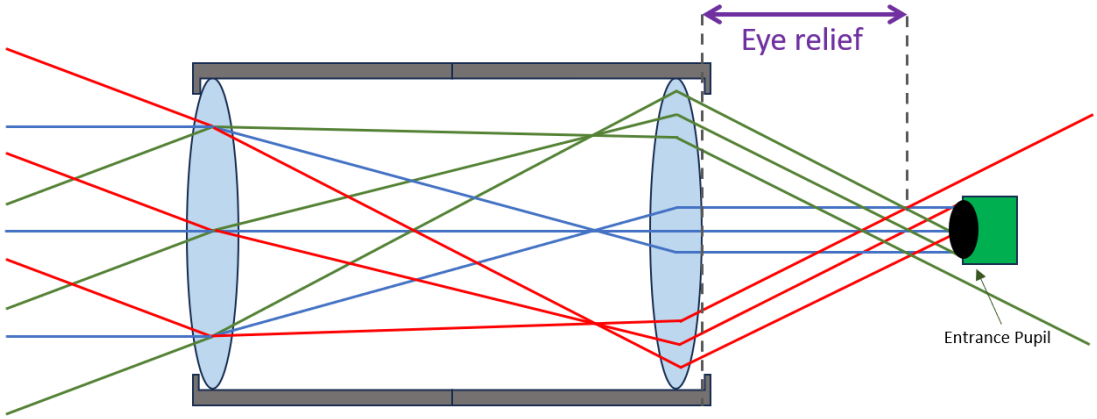

(c) *Axial pupil mismatch*

Figure 2.6. *(a) The exit pupil and the entrance pupil have been aligned and are overlapping. (b) Pupils have been mismatched laterally, but the entrance pupil is still in the eye relief distance. (c) Entrance pupil has been axially displaced.*

2.3 Vignetting and flatfield correction

Vignetting is described as the reduction of the brightness on the edges of the image. Vignetting happens in real-life systems because objects that are off-axis contribute fewer rays in the system. It is mainly an undesired effect that leads images to look very poor on the edges. Especially in optical metrology, where all aberrations and vignetting lead to poor performance, measurement devices are often designed to have minimum vignetting and aberrations. [19] In addition, the measurement instruments are calibrated to compensate for their own aberrations.

Vignetting can also be a direct result of pupil mismatch. In small mismatch, the high field angles are vignetted and thus the image appears to be dimmer on one of the edges than in the center. In an extreme pupil mismatch scenario where the lateral pupil mismatch is larger than half of the exit pupil diameter, the center field is partially vignetted or lost completely. If the vignetting is caused by the axial pupil mismatch then the edges of the image are dimmed or completely lost due to vignetting. This happens because the high field angles will be outside the entrance pupil due to pupil expansion. [8]

Vignetting can be corrected with flat-field correction. The idea is to cancel all unwanted gains coming from the lens and subtract all dark currents of the camera sensor. The flat-field calibration is done pixel-wise. It can be done with very simple math and image processing. The goal of flatfield correction is to have the image to be flat from a uniform light source after correction. [20, 19] The flat-field correction is done with the formula

$$I_{\mathrm{corr}} = \frac{(I_{\mathrm{raw}} - D)F_{\mathrm{max}}}{(F - D)}, \tag{2.4}$$

where I_{raw} is the raw image, D is the dark-frame, F is the flat-field image and F_{max} is the maximum value of $(F - D)$. Flat-field images must be acquired by using very uniform light sources, like integrating spheres. Dark frame images can be taken by blocking light from entering the camera lens or sensor. If we subtract the dark frame from the flat-field image and raw image and calculate the flat-field correction matrix, the Eq. 2.4 can be simplified to

$$I_{\mathrm{corr}} = I_{\mathrm{D}} M_{\mathrm{corr}}, \tag{2.5}$$

where $I_{\mathrm{D}} = (I_{\mathrm{raw}} - D)$ is the dark frame subtracted raw image and $M_{\mathrm{corr}} = \frac{F_{\mathrm{max}}}{(F-D)}$ is flat-field correction matrix. [20] Equation 2.5 can be used with either the mean or the maximum value of the flat-field image. Both of them gives corrected image but with different intensity in different image locations.

2.4 Aberrations

Aberrations in optics refer to the imperfections or distortions that occur when forming an image with an optical system. Aberrations are caused by deviations from ideal behavior which can arise from factors such as lens shape or material. The third-order aberrations are divided into two different categories: Chromatic aberrations and monochromatic aberrations. There are two different chromatic (color) aberrations and five different monochromatic aberrations. [21] One should also note that there are also higher-order aberrations that are outside of the context of this thesis.

The monochromatic aberrations are spherical aberration, Petzval field curvature, coma, astigmatism, and distortion. All of these five aberrations can cause for example image blurring, distortion, and loss of clarity. Chromatic aberrations can be divided into axial chromatic and lateral chromatic which can lead to color fringing. [22]

For example, in AR headsets aberrations may cause nausea, headache, or dizziness to the users. It is very important to test the image quality of the waveguide and detect any aberrations which may cause them to perform poorly. Also, in imaging systems such as cameras, the image quality is desired to be perfect without any aberrations.

These aberrations can be very easily simulated with advanced computer software such as Optalix or Zemax. These optical design applications are easy to use and enable the optimization of very complicated optical systems with minimum aberrations. The optical design tools can be used to calculate and optimize the distances between the lens elements and simulate the aberrations. This enables optical designers to balance aberrations with different lenses and conclude the best lens combination for specific applications.

2.4.1 Spherical aberrations

Spherical aberration happens when light passes through different parts of the spherical lens and focuses on different focal points. This can be seen in Fig. 2.7. It also happens when a spherical mirror reflects light that converges at different focal points.

Spherical aberrations can lead to blurring and reduced sharpness of the image. Optical designers usually counter spherical aberrations by using aspheric lenses as seen in Fig. 2.7. Although, it is much more common to use a technique called "lens splitting", which means that we split a single lens into multiple different lenses that have a total of the same power as the original lens. An example of lens splitting is shown in Fig. 2.8.

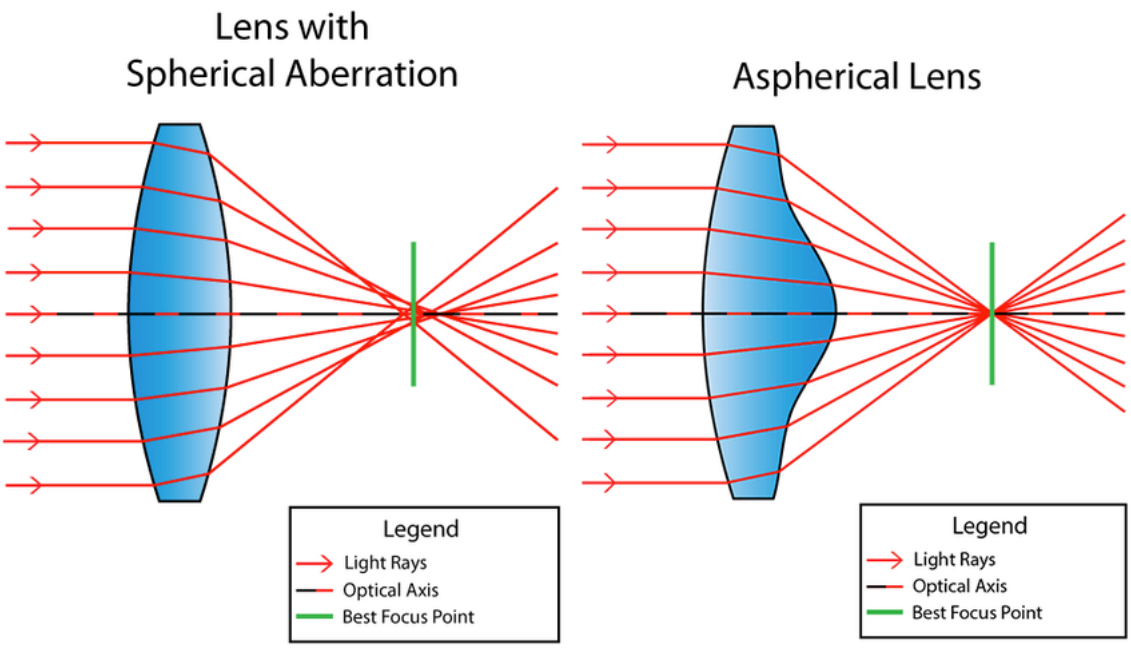

Figure 2.7. *Spherical aberration correction of a normal lens (left) and an aspherical lens (right). [23]*

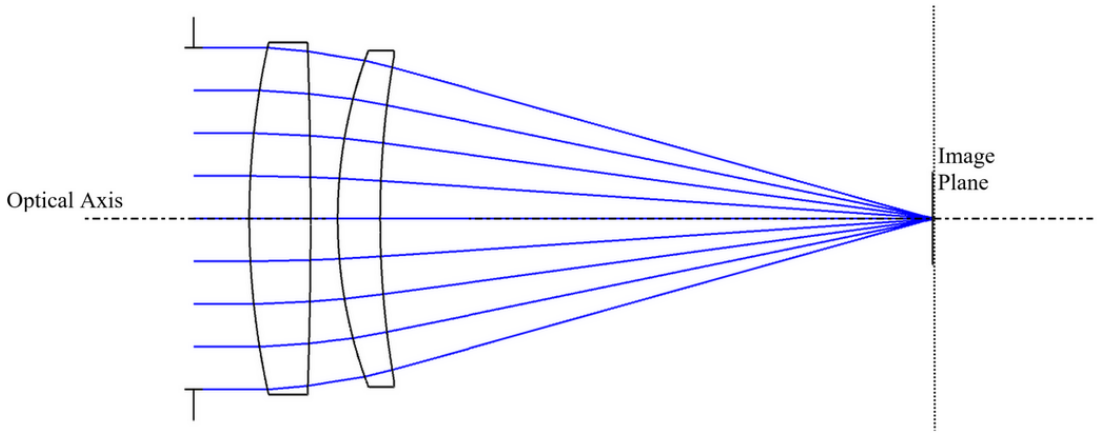

Figure 2.8. *Lens splitting technique used to correct spherical aberration. [22]*

This decreases the angles of incidence while keeping the same power of the lens. Optical designers usually use these techniques with other useful tricks such as reducing the entrance pupil diameter or changing the glass type to a higher index one in order to counter spherical aberration.

2.4.2 Petzval field curvature

Petzval field curvature refers to the optical aberration that is caused by the spherical nature of the lens as the flat object can't be brought to focus on a flat image plane. Even in the absence of other aberrations the image surface of a lens is not truly a plane but rather a curved surface, which is illustrated in Fig. 2.9. This leads images taken with the

camera sensor to be out-of-focus at off-axis locations.[8, 21, 22]

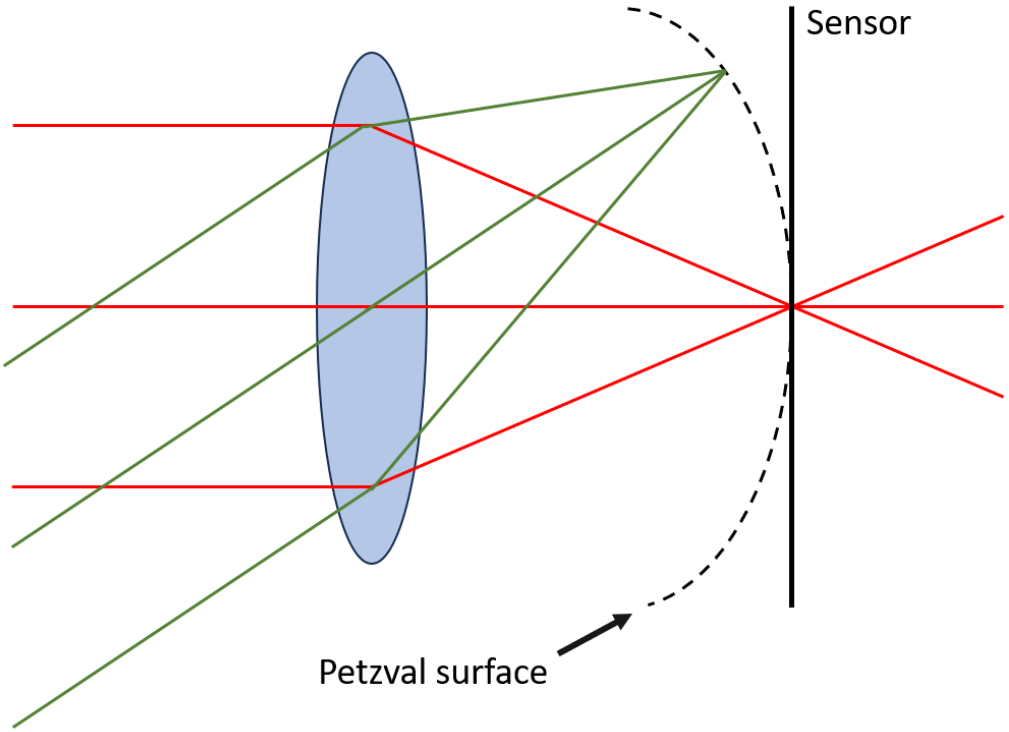

Figure 2.9. *Petzval curvature*

Luckily, there are multiple ways to correct field curvature. The simplest way is to decrease the FOV of the system, but this is not usually possible because optical systems have generally a specific field angle that is desired. Field curvature can be also corrected by using a negative field-flattener lens. The primary way to reduce field curvature is to use extra optical elements which counteract the curved focal plane off-axis. [24] There are also special camera sensors that are curved to compensate for the Petzval field curvature. This kind of curved sensor is not popular as the Petzval curvature is different for each optical system and would require a specific curvature to work with each lens design. [25]

2.4.3 Coma

Coma is an aberration that happens when light rays enter an optical system off-axis and converge at different distances from the optical axis. This is illustrated in Fig 2.10. It leads to smearing and distortion of off-axis points of light in the image. It results in comet-shaped aberration. This distortion is more pronounced towards the edges of the image. [21]

Coma can be minimized with lenses that have the correct shape to match the application. Coma can also be reduced by decreasing the size of the aperture. On the other hand, there are lenses that minimize both the coma and spherical aberrations for a single wave-

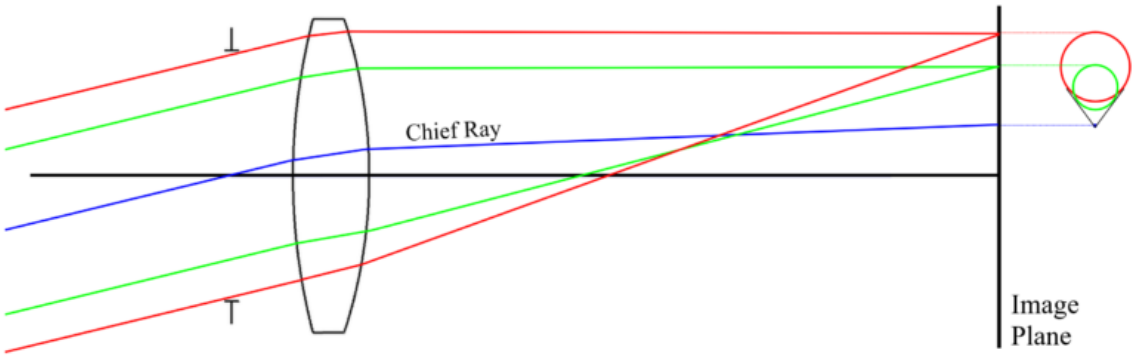

Figure 2.10. *Illustration of the coma on optical system. [22]*

length. They are called best form or aplanatic lenses. Minimizing the coma and spherical aberration requires the lens to meet the sine condition. It states that the ratio of the sine of the finite object angle to the sine of the image angle is constant for all rays. In the case of an infinite object, the infinite object height's ratio to the image angle has to be constant as well. If both of these requirements are met, then the lens is called aplanat. [22] Correcting coma is very important in some applications where precise imaging of objects is essential such as astronomy.

2.4.4 Astigmatism

Astigmatism occurs when the curvature of an optical surface is not uniform in different meridians. It causes light rays to focus at different distances from the optical axis. Basically, this causes the optical system to have two focal positions which are shown in Fig. 2.11. This leads to blurry or elongated images.

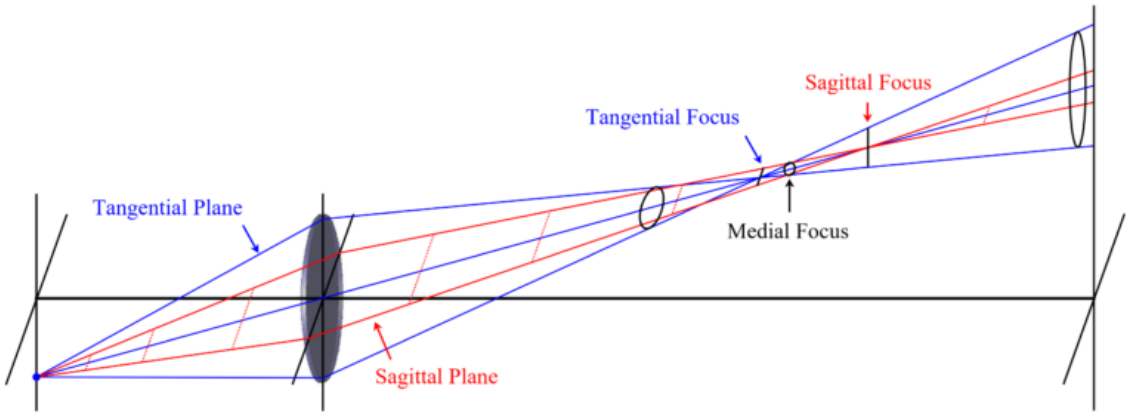

Figure 2.11. *Ray layout of a lens suffering from astigmatism. [22]*

In optical systems, astigmatism can be minimized by optimizing lens elements. Astigmatism is also known for causing human vision to be blurry. It can be corrected with corrective lenses that have different powers in different meridians.

2.4.5 Distortion

Distortion refers to the alteration of the shape or size of objects in an image compared to their actual shape or size. The three types of distortions are barrel distortion, pincushion distortion, and mustache distortion. Distortion can be easily detected just by looking at straight lines through the lens system. If the straight lines appear curved, the system has distortion. Depending on which way the straight lines curve, it can be concluded which type of distortion the system has. Barrel distortion makes the straight lines appear curved outwards and the pincushion distortion makes the lines appear curved inwards. The mixture of these is called mustache distortion. These different distortions are illustrated in Fig. 2.12.

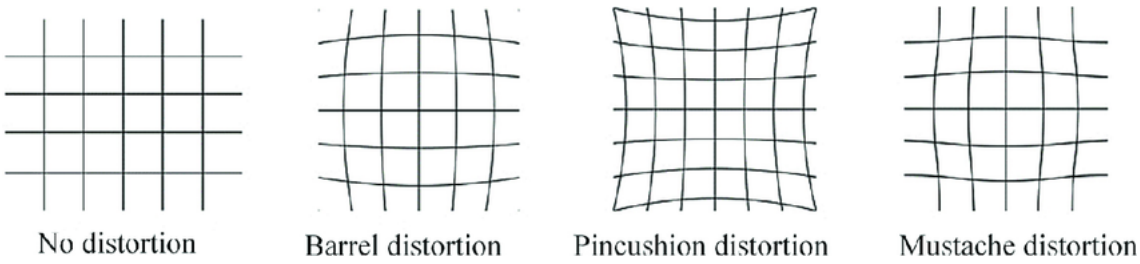

Figure 2.12. *Different types of distortion. [26]*

Distortion can be minimized with lens design. On the other hand, distortion is usually corrected during post-processing of the image. This post-processing requires distortion coefficients separately for each optical system. The coefficients can be acquired during camera calibration or from simulated data. We can use these coefficients to calculate the inverse distortion model and undistort the distorted image. This includes calculating new pixel coordinates for each pixel. For illuminating systems, the distortion can be compensated by pre-distorting the illuminated image. This prevents the illuminated image to be seen as distorted. For everyday applications, such as phones, distortion correction is very essential, because humans are very sensitive to notice any distortion on the images.

2.4.6 Chromatic aberrations

Chromatic aberration is a problem in optical systems where multiple different wavelengths are used. It arises due to the dispersion of light when different wavelengths of light refract differently. For most materials, the refractive index decreases as the wavelength increases. Since the focal length of a lens depends on the refractive index, the focal length will change for different colors of light.

There are two types of chromatic aberrations, which are axial and transverse aberrations. The first one happens when light is focused at different distances from the lens due to different focal lengths. The second one happens when light focuses on different locations in the focal plane. This is caused by the variation in magnification and distortion due to

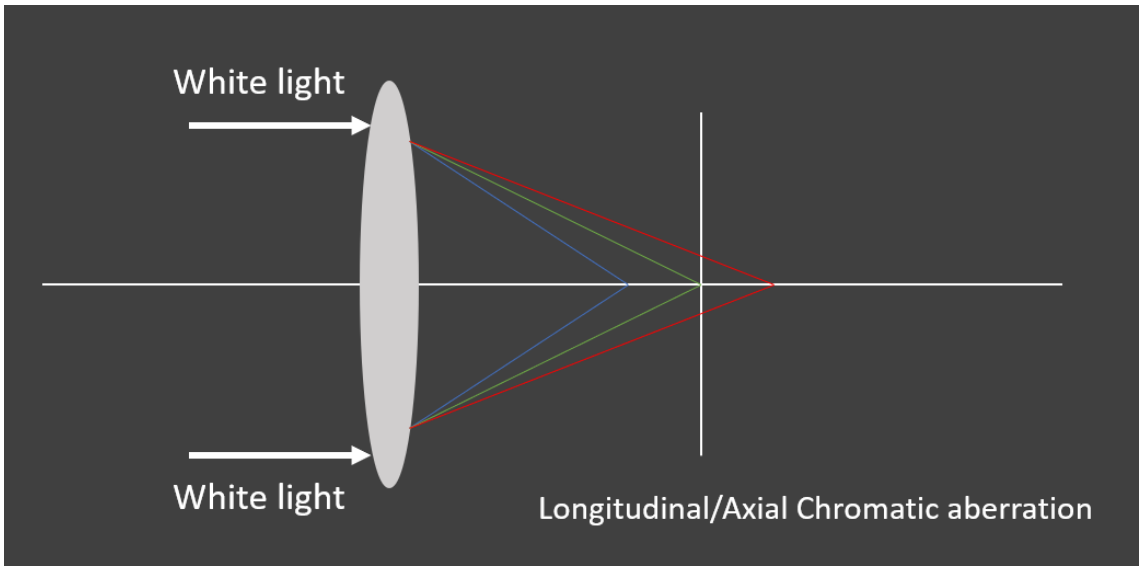

(a)

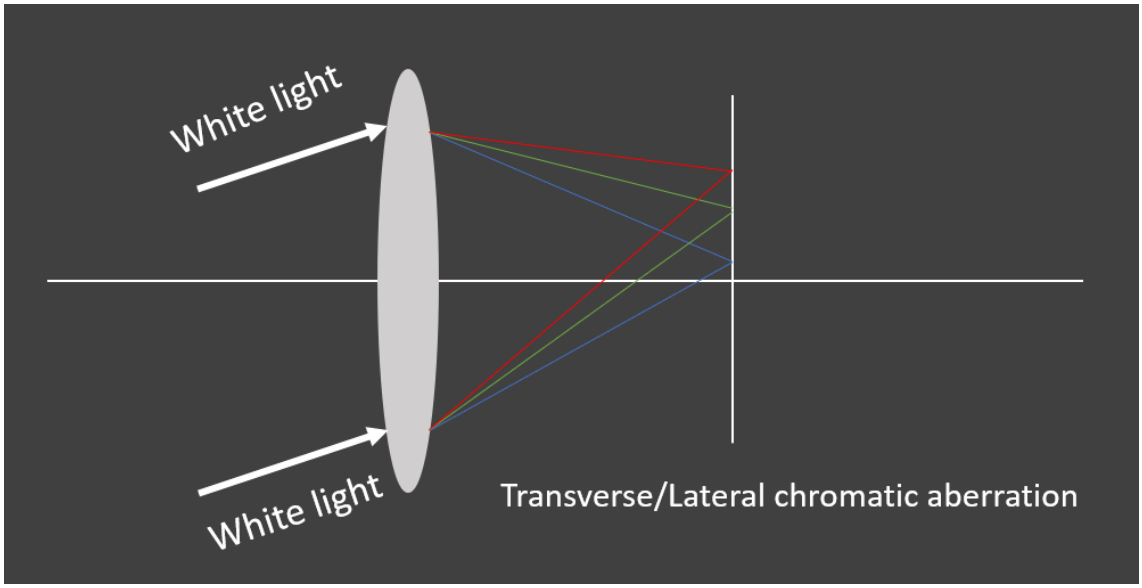

(b)

Figure 2.13. *(a) The green light is focused on the image plane, while the red and blue are focused at different distances. (b) Light coming to the lens in an angle leads to different wavelengths to focus at different positions along the same focal plane.*

different wavelengths. These two different types are presented in Fig. 2.13.

Chromatic aberrations can be compensated with diffractive optical elements, using an achromatic doublet or using apochromatic lens. The apochromatic lens is used to have the same focal length for visible wavelengths but is not regularly used due to its high cost and difficulty to manufacture. In applications where only a single wavelength is required, chromatic aberration is not a problem. Such applications are, for example, laser technology and fiber optics. [12]

2.5 Diffraction

Ray tracing can't be used explicitly when designing optical systems, because it can't explain some of the properties of light. To fully understand different optical phenomena, light has to also be considered as a wave. Huygens-Fresnel principle is a fundamental concept in wave optics. It implies that every point at every given moment on a wavefront acts as a source of secondary spherical wavelets. The new wavefront is the superposition of every single wavelet created at some point, considering its individual phase and amplitude. The sum of these secondary wavelets determines the shape and direction of the wavefront at a later time. [27] It forms the basis for various optical phenomena, such as diffraction and interference, and provides valuable insights into the wave nature of light.

Diffraction is a fundamental phenomenon in wave optics that occurs when waves encounter an obstacle or pass through a narrow opening. According to the Huygens-Fresnel principle, the wavefront bends around the edges of the obstacle or aperture, and this bending of the wavefront is known as diffraction. [28] Diffraction of light is responsible for a variety of optical effects, such as spreading of light around sharp edges, formation of interference patterns in diffraction gratings, and blurring of images in optical systems.

In addition to the bending of wavefronts around obstacles, diffraction is also observed when waves encounter closely spaced structures or when they propagate through regions with varying refractive indices. In such cases, interference of multiple wavelets gives rise to intricate diffraction patterns with regions of constructive and destructive interference. [29] These patterns are observed in a wide range of contexts, including the interference of light waves in Young's double-slit experiment, the diffraction of sound waves around corners, and the diffraction of electrons in quantum mechanics.

One important consequence of diffraction in optical systems is the formation of the Airy disk. When light passes through a small aperture or encounters a diffraction-limited lens, the resulting diffraction pattern forms a central bright spot surrounded by concentric rings of alternating bright and dark regions. [30] This pattern, known as the Airy disk, represents the diffraction-limited point spread function of the optical system. The radius of the Airy disk is

$$r_{\text{Airy}} = 1.22\frac{\lambda}{D}, \tag{2.6}$$

where λ is the wavelength of light used and D is the diameter of the entrance pupil. The Airy disk plays a critical role in defining the resolution limit of the optical system, as it determines the smallest possible spot to which a point source of light can be focused. Diffraction-limited lenses are designed to minimize aberrations and maximize image quality, enabling them to produce images with high resolution and contrast approaching the

theoretical limit set by the Airy disk. [8, 30] Understanding the Airy disk and the diffraction phenomenon is crucial in designing and optimizing high-quality optical systems.

2.6 Contrast and spatial frequency

It is quite difficult to evaluate an optical system's performance because there are many different things affecting it. Therefore optical designers have invented a method to measure an optical system's performance and made it possible to compare different lenses' optical performance to each other. Modulation transfer function (MTF) is a parameter that is used to evaluate the performance of the lens system. It is a standardized way to characterize optical systems. It provides a way to compare different lenses and optimize lens designs. Both contrast and resolution are essential parts of MTF and therefore the image quality. [31]

2.6.1 Contrast

Contrast expresses how well the optical system can distinguish white and black areas. One way to define it is luminance contrast, which is defined as the ratio of luminance difference between maximum and minimum luminance and the average luminance. There is also Weber contrast, which uses the luminance of the background and features to calculate the contrast. The most commonly used metric for contrast is the Michelson contrast. It can be calculated with

$$C = \frac{I_{\max} - I_{\min}}{I_{\max} + I_{\min}}, \tag{2.7}$$

where $I_{\max}$ is the maximum intensity of the object and $I_{\min}$ is the minimum intensity of the object. It is illustrated in Fig. 2.14.

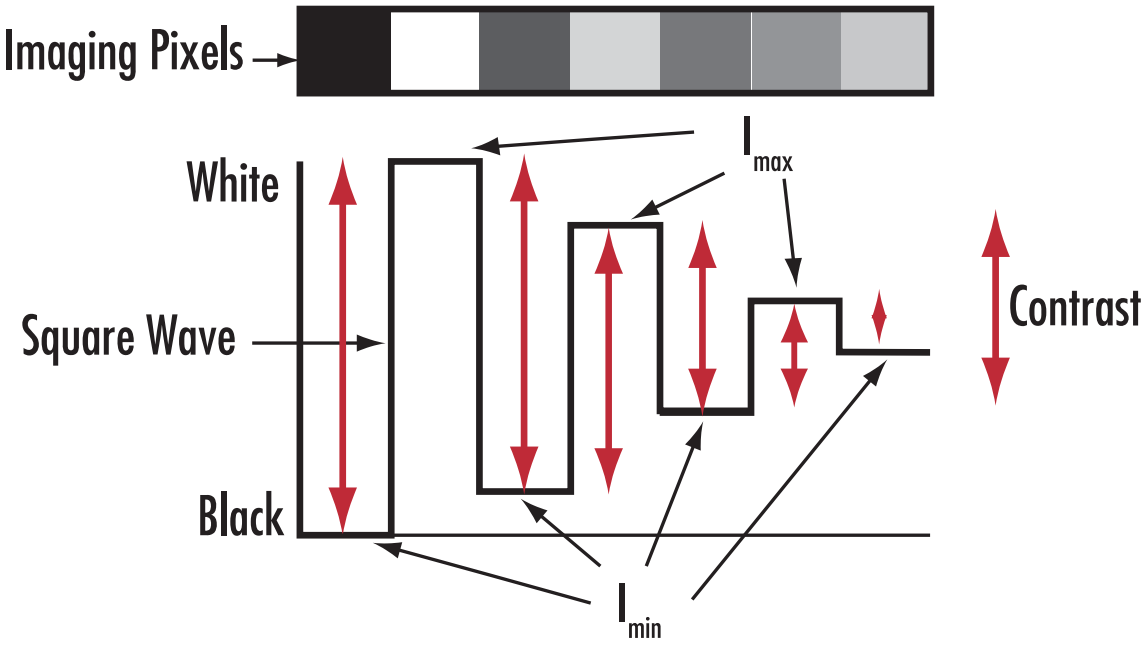

Figure 2.14. *Transition from black to white is high contrast while intermediate greys indicate lower contrast [32]*

On the other hand, there are different ways to calculate the contrast for projectors, TVs, and waveguides. One way to measure contrast for this kind of application is FOFO (Full On/Full Off) contrast which measures bright and dark pixel values when the light is on and off separately. Another way to measure contrast is to use American National Standards Institute (ANSI) contrast which uses a checkerboard and measures the dark and bright pixel values simultaneously. More on this in Chapter 3. Because there are many different definitions for contrast, it is almost impossible to compare different publishers' results [33]. For example, in some applications such as TVs and monitors the contrast is calculated by dividing the bright pixel value by the dark pixel value. This can lead to infinite contrast because the OLED (Organic Light Emitting Diode) panels have individual pixels that can turn on and off resulting in 0 intensity in dark pixels. For comparison, the Michelson contrast can get values only between 0 and 1.

2.6.2 Resolution

On the other hand, contrast alone doesn't make the image look good. It also needs to have a high enough resolution. Resolution means the ability to transfer the details. In imaging systems, this means how well the optical system can reproduce object details. The smaller details the optical system can reproduce the better resolution it has. One should also note that resolution is only meaningful when the contrast is specified [32]. In the consumer applications such as monitors or camera sensors, the resolution is defined as the number of pixels in rows and columns. This definition is enough for consumer applications, but it isn't the complete description of the resolution. Resolution can be

defined as the minimum size that is resolvable by a lens or system. Therefore resolution is defined with the spatial frequency which is measured in line pairs per millimeter. This definition can be applied to camera sensors as we know the pixel size.

One of the most important definitions is the Nyquist frequency which means the highest frequency resolvable by a sensor. It is defined as one line pair or 2 pixels. This is usually called the resolution of the sensor or referred to as the system's image space resolution and it is calculated as

$$\xi_{\text{sensor}} = \frac{lp}{2s}, \tag{2.8}$$

where lp is the line pair and s is the pixel size in millimeters. Directly from Eq. 2.8, one can notice that the larger the pixel size the smaller the image space resolution is.

The reason why resolution can't be defined only with pixel dimensions lies in the nature of light. When light transmits through any size aperture, diffraction occurs. [30] This results in the diffraction pattern, a bright spot in the center, and a series of rings of decreasing intensity around it. This can lead to two light dots to be indistinguishable from each other if they are placed close enough together. Fig. 2.15 shows how the Airy disks merge when two single-point light emitters are moved closer to each other.

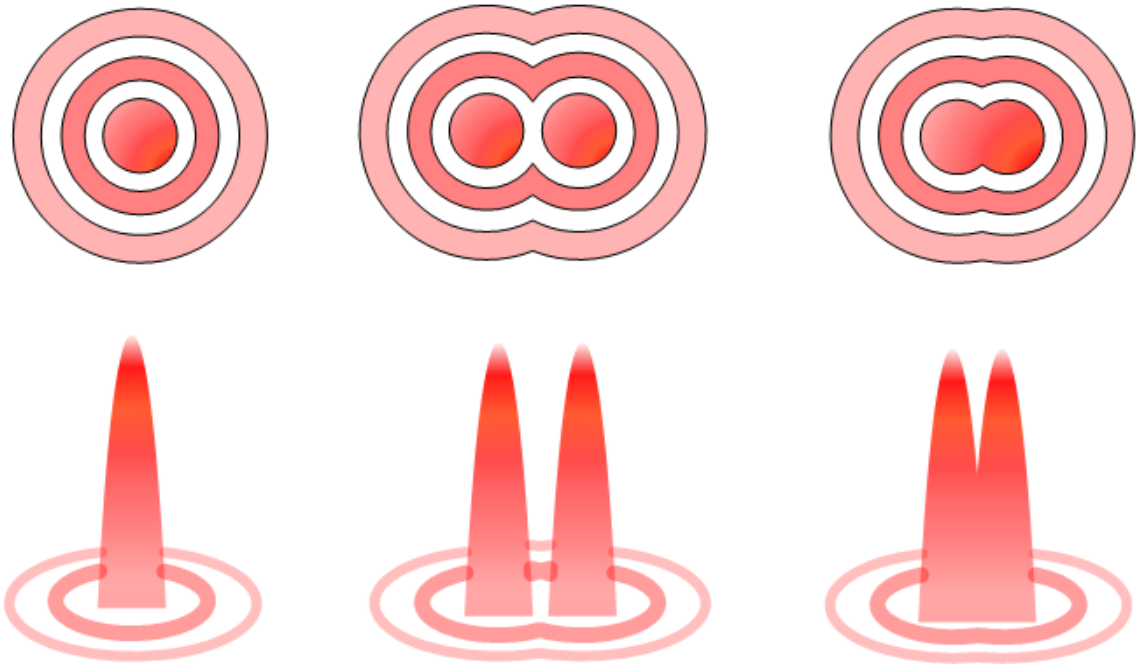

Figure 2.15. *Single Airy disk (left), two Airy disks next to each other (middle) and two Airy disks moved closer to each other are indistinguishable from each other. [34]*

This limitation in the optical performance of the optical system is called the diffraction limit. It gives the maximum theoretical resolving power in line pairs per millimeter. Even a perfect lens is limited by it. This limit is defined as the point when two airy disks are

no longer distinguishable from each other. This limits the resolution of the optical system and this limited resolution is often called cutoff frequency. It can be calculated using the lens's f-number and wavelength of the light with

$$\xi_0 = \frac{1}{\lambda(f/\#)}, \tag{2.9}$$

where $f/\#$ is the f-number of the lens and λ is the wavelength of the light.

2.6.3 Modulation transfer function

The MTF curve is a graphical way to show the optical system's performance. The MTF graph reflects how a lens reproduces contrast as a function of spatial frequency (resolution). Basically, it measures a lens's ability to transfer the contrast of an object to an image using spatial frequency. This curve shows how the optical aberrations and other parameters affect the lens performance. The diffraction limit can also be shown in the graph to illustrate the maximum theoretical performance for a specific lens. This is how optical designers can optimize their lens designs. Spatial frequency indicates the number of line pairs per millimeter (lp/mm) or cycles per millimeter (cycles/mm). Generally, various charts shown in Fig. 2.16 are used to measure the MTF of a lens. They are usually alternating black and white lines with equal spacing or simple slanted edges. The MTF can also be calculated by using a crosshair pattern.

In general, MTF is the best way to analyze the performance of the optical system in terms of contrast and resolution. The MTF enables an easy way to show the optical system's contrast, resolution, and aberrations at the same time. It can be used to determine if an optical system is feasible or not for a specific application. It can also be used to show how well a lens performs in a single chart. It is a standardized method to qualify optical systems and applications as it makes it easy and fast to compare two different designs' performance.

Whenever we want to plot the MTF graph we have to calculate the MTF at every spatial frequency. For an ideal optical system with a circular pupil, the ideal MTF is

$$\mathrm{MTF}(\xi) = \frac{2}{\pi}\left(\arccos(\frac{\xi}{\xi_0}) - (\frac{\xi}{\xi_0})\sqrt{1-(\frac{\xi}{\xi_0})^2}\right), \tag{2.10}$$

where ξ_0 is the cutoff frequency shown in the Eq. 2.9. Although the MTF of any optical system can be calculated with modern optical design tools, the real-world performance might differ from that. This is due to manufacturing tolerances and errors which can lead to varying performance. Because all of the components have their own MTF, they all contribute to the overall MTF of the system. This way the weakest link of the system is

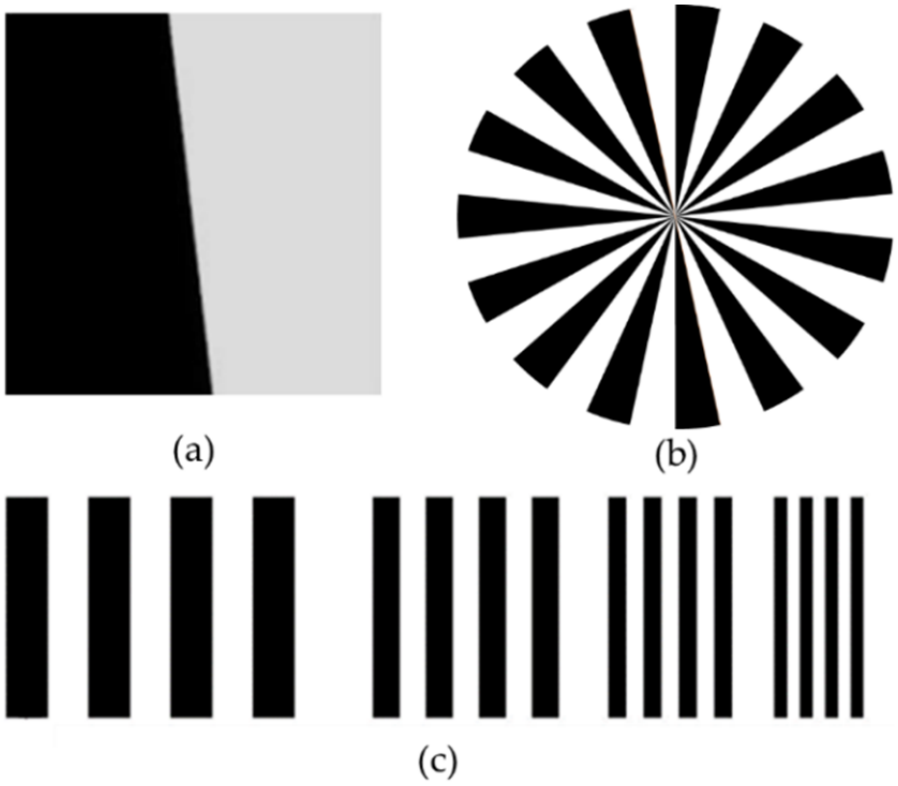

Figure 2.16. *a) Slanted-edge pattern, b) Siemens star pattern, c) Sinusoidal pattern. [35]*

not the limiting factor, but the overall system. This helps optical designers to design better and more efficient new optical systems with specific requirements. [36]

3. WAVEGUIDE IMAGE QUALITY TESTING

In the AR industry, companies are currently making substantial investments in the development and rigorous testing of their products. The manufacturing process, while not yet in mass production, is undergoing continuous refinement as companies seek effective means to assess the image quality of their AR glasses. The AR industry is still in the research and development phase, during which different companies are actively producing prototypes of their AR glasses and exploring diverse technological solutions. Given the intricate and time-consuming nature of AR glasses production, many companies are engaging in collaborations and partnerships. For instance, individual firms may focus on specific components or functionalities within the AR glasses manufacturing process. These may include producing the glass for the waveguide, implementing gratings on the glass, developing the light engine, conducting the assembly, or overseeing the software integration. These intercompany collaborations share the expertise and resources, leading to a more efficient and concerted advancement of AR technology.[37]

In the domain of AR glasses, the waveguide serves as a critical component responsible for guiding virtual images produced by the light engine to the user's eye. The manufacturing process of these waveguides involves several intricate steps, and at each stage, manufacturers seek to evaluate the performance and image quality of their product. These image quality measurement steps encompass wafer-level assessments, evaluations of cut and shaped waveguides, and final assembly inspections of AR glasses' image quality and overall performance.[38]

Wafer-level measurements include evaluating essential parameters such as grating period and orientation using a Littrow diffractometer while employing an image quality measurement system to conduct comprehensive image quality tests. Subsequently, cut and shaped waveguides undergo rigorous assessments to gauge parameters such as contrast, FOV, distortion, and MTF, among others. Finally, the assembled AR glasses undergo quality control evaluations, during which their respective light engines are utilized to gauge overall performance. These assessments encompass image quality tests, photon-to-photon latency evaluations, and eye-tracking testing. [39]

In this thesis context, we are specifically interested in evaluating the image quality of the waveguides within the AR glasses. As such, our focus is on the optical properties

and performance of the waveguides, which play a crucial role in delivering the AR visual content to the user's eyes. However, before delving into the intricacies of image quality analysis metrology, it is important to understand the fundamental functioning principles of AR glasses.

3.1 The main principles of augmented reality displays

The basic principle of AR display is to produce a virtual image in the user's field of view without disturbing the view of the real world. This means that the AR waveguide must be transparent and ideally should not cause any aberrations in the view of the real world. There are 3 different types of designs for AR glasses which are free-space combiners, freeform total internal reflection prism combiners, and waveguide combiners.[18, 40] We are mainly focusing on the waveguide combiners although some of the things discussed in this chapter can be applied to the other types as well. An optical waveguide is a piece of glass that guides the light inside of it using TIR which was discussed in Chapter 2. [40, 41]

When conducting image quality tests for a waveguide, a comprehensive understanding of its operational principles is imperative. Waveguides exhibit dual functionalities, operating in either reflection or transmission modes contingent upon their specific design, as depicted in Fig. 3.1. For instance, Microsoft Hololens 2 uses a transmission mode, given that its light engine is situated on the opposing side relative to the user's eye. [42] Conversely, the Magic Leap 2 is configured to function in reflection mode, with the light engine located on the same side as the user's eye. [43]

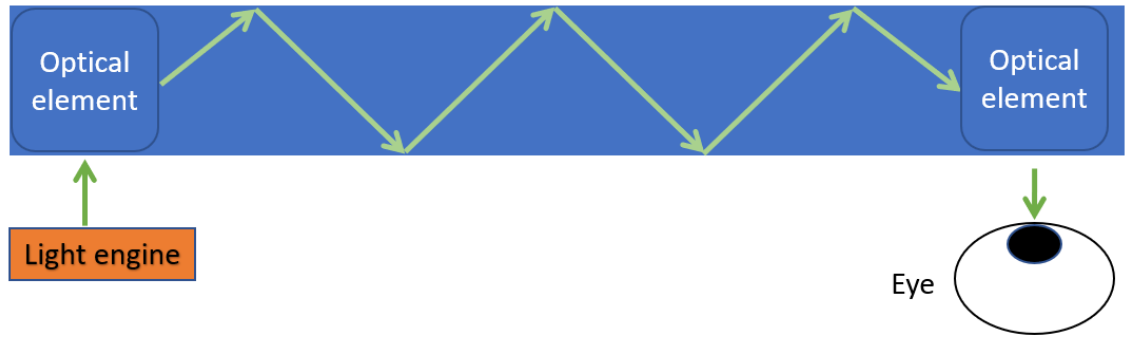

(a) *Reflection mode*

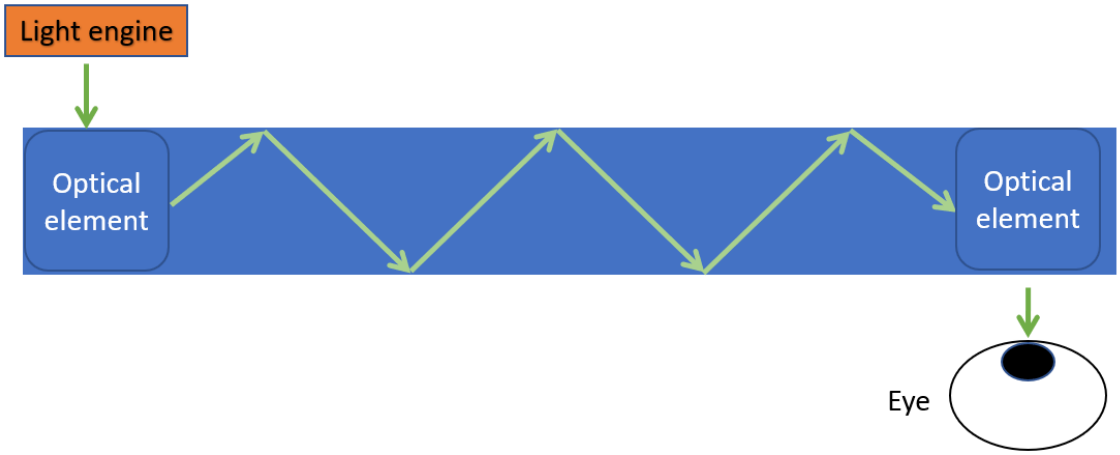

(b) *Transmission mode*

Figure 3.1. *(a) Reflection mode. The user's eye and the light engine are on the same side of the waveguide (b) Transmission mode. The light engine and the user's eye are on the opposite sides of the waveguide.*

Waveguide structures are categorized into four distinct types: reflective, polarized, diffractive, and holographic waveguides. Each category encompasses particular advantages and drawbacks that extend beyond the confines of this thesis. Nevertheless, the fundamental objective across all waveguide structures remains consistent – to guide light through the waveguide to the user's eye utilizing TIR and superimpose a virtual image onto the real-world environment. [44]

3.2 Image quality of waveguide

In the design of AR glasses, various considerations play a crucial role in optimizing the user experience. Among the paramount factors contributing to an ultimate AR experience are comfort and immersion. Comfort, being a subjective concept, is contingent upon individual preferences and prior exposure to similar headsets or glasses. To ensure user comfort, AR glasses must feature wearable and vestibular comfort attributes, as well as account for visual and social comfort aspects. A small, lightweight, and well-designed headset is essential to minimize discomfort, avoiding pressure points that may cause

headaches or nausea. Visual comfort features include a large eye box to accommodate varying interpupillary distances, eye tracking, excellent angular resolution, high contrast, and high brightness, among other considerations. Immersion, an equally critical aspect of the AR experience, is influenced by visual comfort features and augmented by additional attributes, including a large FOV, gesture sensing, and motion-to-photon latency. [18]

To enhance image quality and deliver a more immersive experience, companies are continuously refining their AR glasses. Image quality measurements for waveguides are very significant, as even an optically well-designed waveguide may still be affected by manufacturing and assembling errors, compromising image quality. Manufacturers seek to benchmark their waveguides against competitors, and standardized image quality testing plays an important role in achieving this objective. Numerous standards are available for companies to adopt, such as those established by the American National Standards Institute (ANSI), the International Electrotechnical Commission (IEC), the International Organization for Standardization (ISO), and the Society for Information Display (SID). [45, 46, 47, 48] Companies may choose to follow any standard that suits their preferences, but the multitude of standards introduces complexity in comparing results. Consequently, waveguide image quality testing demands careful consideration of the chosen standard to ensure meaningful and comparable measurement results.

3.2.1 Contrast

As discussed before in Chapter 2, contrast plays an important role in how crisp and sharp images look. Consequently, manufacturers of AR glasses seek to evaluate the contrast of their waveguides to ensure optimal visual performance. One commonly used method to calculate waveguide contrast involves illuminating a checkerboard pattern onto the waveguide and subsequently capturing the output image. The checkerboard pattern may vary in size, with standards such as ANSI utilizing 4 x 4 checkerboards and ISO employing 5 x 5 checkerboards, as depicted in Fig. 3.2. [49] Furthermore, it is relevant to acknowledge that checkers don't need to be confined to squares as they may also be in the form of rectangles, wherein their width and height don't need to be equal. This versatility provides further flexibility in conducting comprehensive contrast evaluations, containing various geometries to account for the diverse optical characteristics of waveguides. The ANSI contrast measurement, owing to its utilization of an even number of checkers, yields an equal number of dark and bright checkers, making it a popular choice for evaluating the contrast of different applications. This technique offers a reliable means to quantitatively assess the waveguide's ability to reproduce differences in luminance, thereby aiding manufacturers in optimizing their product's image quality.[50, 51, 52]

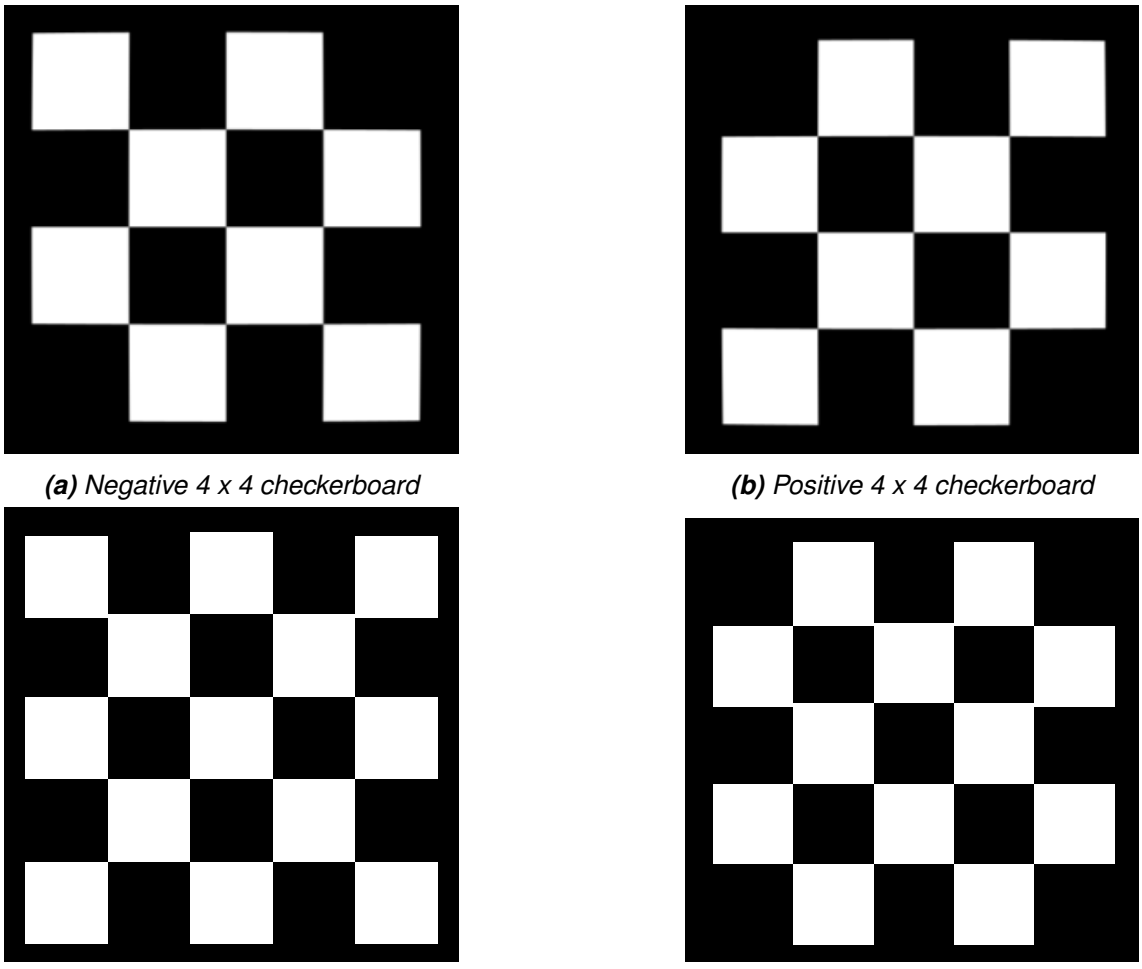

(a) *Negative 4 x 4 checkerboard*

(b) *Positive 4 x 4 checkerboard*

(c) *Negative 5 x 5 checkerboard*

(d) *Positive 5 x 5 checkerboard*

Figure 3.2. *(a) ANSI standard 4 x 4 negative checkerboard (b) ANSI standard 4 x 4 positive checkerboard.*

The ANSI contrast is calculated from a 4 x 4 checkerboard image by determining the average luminance of the bright and dark squares. By considering the interaction of light from the bright and dark regions, the ANSI contrast provides insights into the optical system's performance in real-world scenarios. The results obtained show how the waveguide functions under practical usage conditions when presenting content. By quantifying the contrast levels between bright and dark elements in the displayed image, the ANSI contrast measurement offers valuable information for optimizing the waveguide's image quality. The ANSI contrast ratio can be calculated as

$$C = \frac{L_{\mathrm{Bright}}}{L_{\mathrm{Dark}}}, \tag{3.1}$$

where L_{Bright} is the bright average luminance and the L_{Dark} is the dark average luminance of the checkerboards. Note that in an ideal case, the dark squares would be totally black meaning zero intensity leading to infinite contrast. But in real-world scenarios that

is impossible due to the limitations of materials and hardware.

The contrast ratio measurement can offer diverse interpretations, as companies have the flexibility to utilize varying checkerboard configurations with differing square densities to calculate contrast. This versatility becomes particularly advantageous for waveguides, as the checkerboard pattern allows for contrast calculations at any field location. This process involves dividing the intensity value of each bright square by the average intensity of the four adjacent dark squares. An alternative method entails employing both negative and positive checkerboard patterns, capturing images of each, and subsequently dividing the images to calculate contrast.

By adopting such methodologies, the evaluation of the waveguide's performance is not restricted solely to the center of the image but extends to the edges of the image as well. The contrast can be assessed at various locations within the FOV. This comprehensive approach leads to a detailed analysis of the waveguide's contrast performance throughout the entire FOV, enabling manufacturers to gain valuable insights into the optical system's behavior under diverse viewing conditions. By evaluating contrast in multiple field locations, designers and engineers can optimize the waveguide's performance across the entire display area, ensuring a consistently high-quality visual experience for users of AR glasses.

The contrast ratio value in the ANSI method is dependent upon the size of the checkerboard used. Notably, the ANSI contrast is specifically defined for a 4 x 4 checkerboard configuration. However, if denser squares are employed, such as a 10 x 10 checkerboard, the contrast performance may decrease in comparison to larger checker sizes.

The size of each checker is measured as an angle within the FOV. For instance, in a waveguide with a 40° x 40° FOV using the ANSI checkerboard, each checker will have an angular size of 10° x 10°. However, this representation may not fully correspond to real-world scenarios, as the checker size is relatively large. To address this limitation and achieve a more precise assessment, companies may use denser checkerboard patterns, reducing each checker's angular size to, for example, 1°. In the context of a 40° x 40° FOV, this would require using a 40 x 40 checkerboard configuration. Such modifications enable the evaluation of performance at different field locations, allowing for the calculation of contrast non-uniformity as

$$\mathrm{CNU} = \frac{C_{\max} - C_{\min}}{C_{\mathrm{avg}}}, \tag{3.2}$$

where $C_{\max}$ is the maximum contrast ratio among the checkers, $C_{\min}$ is the minimum contrast ratio among the checkers and C_{avg} is the average contrast ratio. Generally, the high contrast ratio indicates high image quality and lack of stray light.

3.2.2 Uniformity

In the context of image quality evaluation, the term "uniformity" encompasses various aspects, including luminance uniformity, luminance non-uniformity, chromaticity uniformity, and chromaticity non-uniformity. Although the terms "luminance uniformity" and "luminance non-uniformity" are often used interchangeably, a subtle distinction exists between them. Luminance uniformity pertains to the degree of consistency in luminance levels across the FOV at different field locations. On the other hand, luminance non-uniformity quantifies the extent to which luminance values deviate from uniformity within the FOV. In practice, luminance uniformity measurements are predominantly conducted using the solid reticle pattern illustrated in Fig. 3.3. However, the 5 x 5 negative checkerboard depicted in Fig. 3.2c may also be utilized for this purpose. These patterns offer reliable means to assess the consistency of luminance distribution across the FOV and are instrumental in evaluating the overall visual performance and quality of waveguides used in AR glasses.

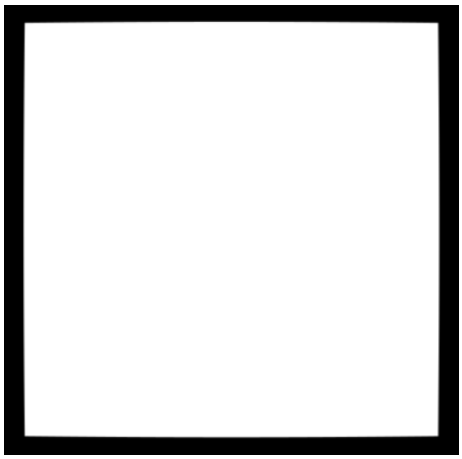

Figure 3.3. *Solid reticle pattern.*

The luminance non-uniformity can be calculated according to the IEC-63145-20-10 standard, using

$$\mathrm{LNU} = \frac{L_{\max} - L_{\mathrm{avg}}}{L_{\mathrm{avg}}} 100\%, \tag{3.3}$$

where $L_{\max}$ is the maximum luminance value and L_{avg} is the average luminance value across the defined field locations. These defined measurement locations (P_0 to P_8) are shown in Fig. 3.4 and the average luminance value is calculated with

$$L_{\mathrm{avg}} = \frac{1}{N} \sum_{i=1}^{N} L_{P_i}, \tag{3.4}$$

where L_{P_i} is the luminance value at specific measurement location P_i.

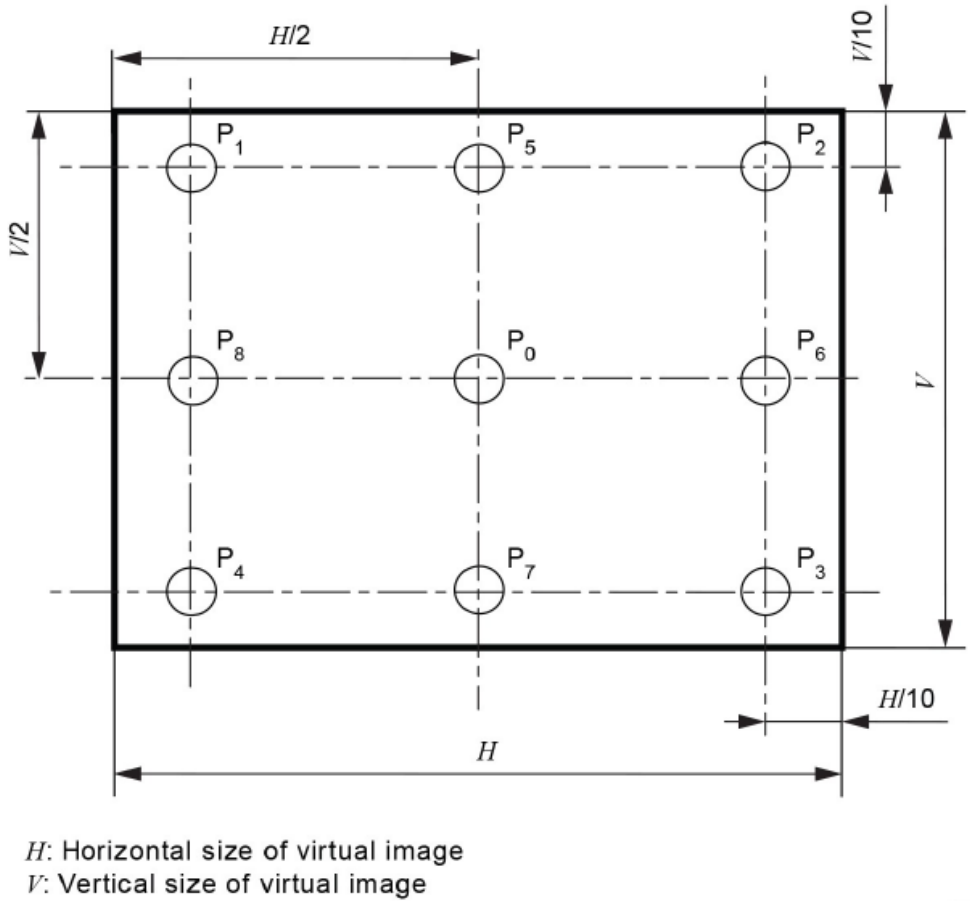

Figure 3.4. *Measurement locations (P_0 to P_8) according to the IEC 63145-20-10.[49]*

Chromaticity uniformity refers to how well the chromaticity remains constant across the FOV of the object. Alternatively, chromaticity non-uniformity characterizes how the chromaticity varies across the surface of the screen. [52] This chromaticity uniformity is measured in the CIE 1976 UCS chromaticity coordinates (u'_i, v'_i) which are calculated from the CIE 1931 chromaticity coordinates (x_i, y_i)

$$u' = \frac{4x}{-2x + 12y + 3}, \text{ and} \tag{3.5}$$

$$v' = \frac{9y}{-2x + 12y + 3}, \tag{3.6}$$

These CIE 1976 chromaticity coordinates are then used to calculate the chromaticity distance between pairs of sampled colours using

$$\Delta u'v' = \sqrt{(u'_j - u'_i)^2 + (v'_j - v'_i)^2}, \tag{3.7}$$

where $i,\ j$ =0 to 8 and $i \neq j$. The chromaticity non-uniformity is defined as the largest sampled chromaticity distance between any two points. [49] The current approach to uniformity measurements employs sampled uniformity, wherein discrete locations on the display are utilized to calculate uniformity and non-uniformity metrics. This methodology facilitates quick data analysis. However, it may not always provide a comprehensive representation of uniformity across the entire FOV. Conversely, the full field uniformity can be analyzed through area uniformity assessment, wherein the entire measurement image is considered, necessitating computation for each individual pixel value as a separate measurement location. While area uniformity offers a more comprehensive evaluation of uniformity characteristics across the entire FOV, its application demands considerably higher computational resources. Therefore, the choice between sampled uniformity and area uniformity depends on the specific objectives of the evaluation and the available computational capacity. Each method offers unique insights into the waveguide's performance, enabling a comprehensive understanding of its uniformity attributes and contributing to the ongoing advancement of AR glasses technology.

3.2.3 Field of View and image rotation

The FOV of an AR headset is a critical property for achieving an immersive AR experience. Consequently, waveguide FOV is of significant interest to manufacturers aiming to provide a large FOV with minimal side effects. Measuring the FOV of a waveguide can be accomplished using any reticle as long as the entire reticle is visible. However, there are instances where the waveguide may not produce a satisfactory image, resulting in the corner points of the reticle being obscured. To address this, the most prevalent method for calculating FOV involves illuminating a solid reticle onto the waveguide.

A predetermined cap value, such as 50 percent, can be utilized in the analysis, identifying the points in the x and y directions where the intensity of light drops below 50 percent of the center pixel light intensity. This follows the standard IEC 63145-20-10:2019. An example of an analyzed image is illustrated in Fig. 3.5. If the image is clear enough, the corner points of the solid reticle can be detected and the FOV can be calculated directly from those pixel coordinates. The foundation of the FOV measurement lies in the knowledge of the camera's angular resolution and the angular map derived from distortion calibration. This enables the calculation of the angle of the reticle from the pixel coordinates, allowing for accurate FOV determination.

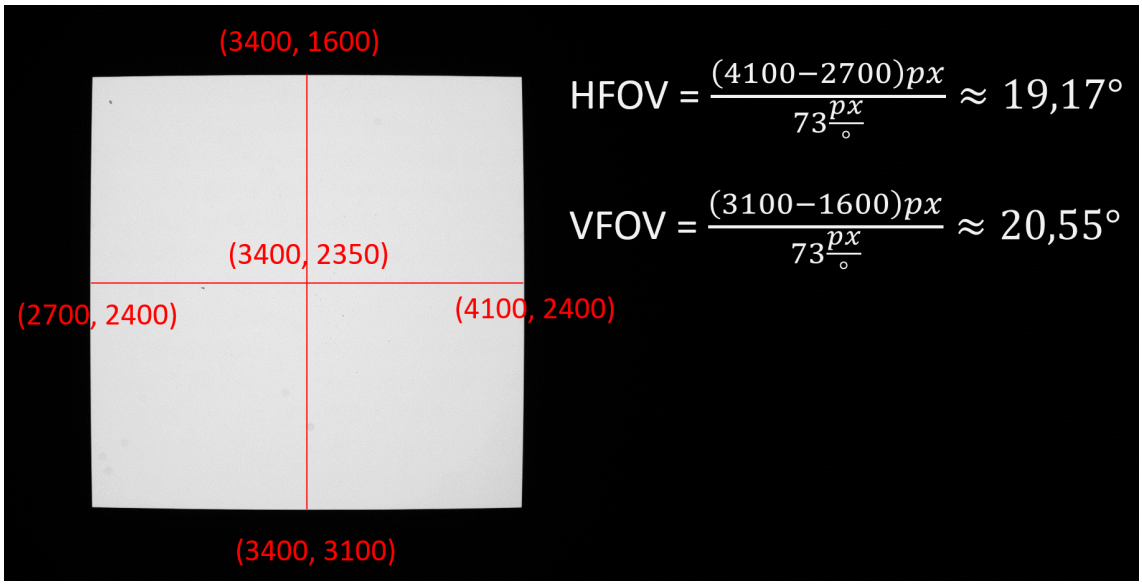

Figure 3.5. *Field of view analysis showing the horizontal and vertical field of view.*

The image rotation can also be determined using the solid reticle. By detecting at least two corner points of the solid reticle pattern, a line can be drawn between these points, and the slope of that line is utilized to ascertain the image rotation. However, it is important to acknowledge that this slope can vary depending on the reticle orientation or waveguide design. Consequently, the reference orientation of the reticle has to be known to ensure an appropriate evaluation of image rotation through the waveguide.

3.2.4 Efficiency

Although not directly associated with image quality, waveguide efficiency is undeniably one of the most crucial aspects of waveguide performance. An exceptional waveguide efficiency holds the promise of enabling smaller and more energy-efficient AR glasses, as the light engine would require less energy to illuminate the image. This efficiency gain would lead to reduced battery size or prolonged battery life, thereby contributing to a more compact and portable device form factor. Consequently, the measurement of waveguide efficiency is very important for waveguide manufacturers. Fortunately, the efficiency of the waveguide can be assessed using the same image quality measurement system employed for image quality properties.

The waveguide efficiency is quantified as a measure of how effectively the waveguide transmits light from the input to the output. Given that efficiency is a relative value, the solid reticle, depicted in Fig. 3.3, can be utilized to measure it. The efficiency measurement involves capturing both a reference image and a measurement image. Subsequently, the reference image is divided by the measurement image to derive the efficiency value. This produces pixel-wise efficiency values between 0 and 1.

However, an inherent challenge lies in accounting for exposure time differences, as the intensity of light is different between reference and measurement images, and exposure time is changed according to the intensity of light. To address this issue, exposure linearity dependency is employed during camera calibration. This process allows for compensation of exposure time changes in the measurement image, ensuring accurate and reliable efficiency assessments. An alternative method is to use a known neutral density (ND) filter during the reference measurement to decrease the intensity of light. The ND filter is chosen so that the exposure time would be similar between a reference image and a measurement image. This method requires knowing the exact efficiency of the ND filter for each wavelength. The efficiency of the ND filter can be calculated by measuring the power without the ND filter and with it. The correction coefficient is calculated then by dividing the power values by each other. Then the reference image's each pixel value is multiplied by this coefficient before calculating the efficiency.

3.2.5 Evaluation of modulation transfer function

MTF is used to evaluate the waveguide's performance in terms of spatial resolution and image sharpness. The MTF performance of a waveguide is measured using a slanted edge, crosshair, or similar pattern shown in Fig. 2.16. The two most commonly used patterns are crosshair and slanted edge which are shown in Fig. 3.6.

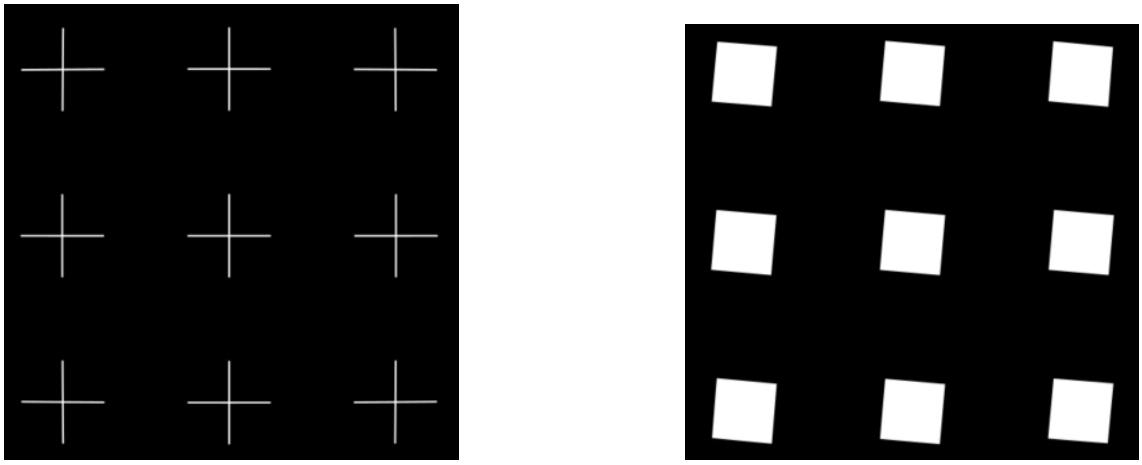

(a) *Crosshair pattern* ***(b)*** *Slanted Edge pattern*

Figure 3.6. *(a) Crosshair pattern (b) Slanted Edge pattern*

The MTF analysis entails calculating the MTF performance separately for each slanted edge or cross, enabling simultaneous measurement of the MTF across different sections of the FOV. The procedure for determining MTF performance is similar for both patterns.

To conduct MTF analysis from a crosshair image, the line spread function (LSF) is acquired for each arm of each cross. Subsequently, a fast Fourier transform (FFT) is applied to these LSF values, enabling the plotting of the MTF-spatial frequency graph. The

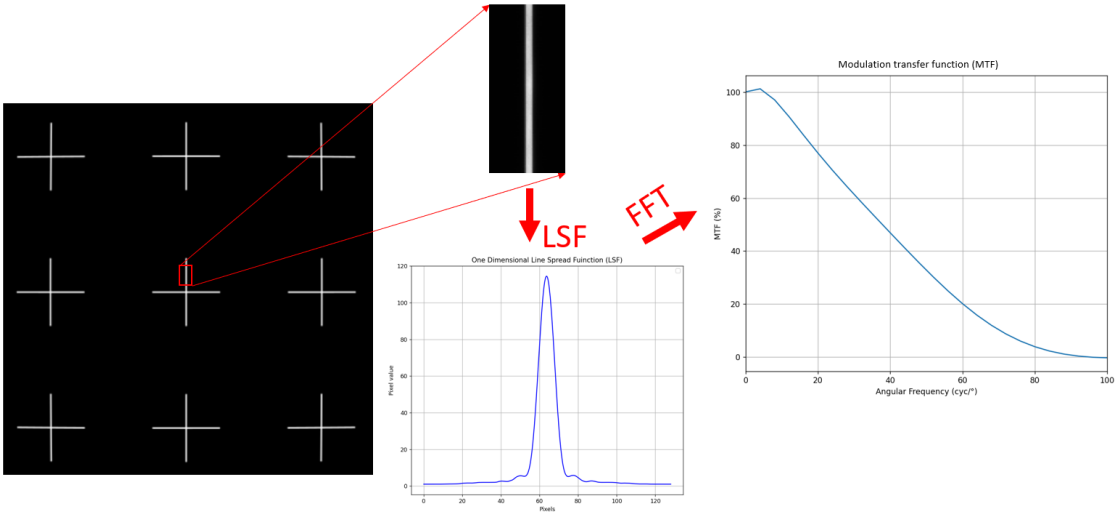

Figure 3.7. *Evaluation of line spread function and modulation transfer function from crosshair. The same process can be done for all arms of each cross to calculate the total MTF performance over the whole FOV.*

process involves calculating the MTF as a function of horizontal and vertical spatial frequency, as illustrated in Fig. 3.7.

However, the crosshair pattern has a significant drawback since it is very sensitive to image rotation. Notably, the MTF values experience noticeable reductions when the orientation of the cross changes. Consequently, the slanted edge pattern is more commonly employed, despite its more complex analysis.

For slanted edge analysis, the ISO12233 standard is widely adopted. This standard employs a slanted edge oriented at an angle of approximately 4-6 degrees from the vertical direction, allowing the gradient of the edge to be measured at various phases relative to the photo elements of the image sensor. [53] It also allows a slight image rotation in the image. The first step in analyzing the MTF of the slanted edge is calculating the edge spread function (ESF). It describes how the intensity changes across the transition from one side of an edge or line to another in an image. The ESF is essentially a plot of the pixel intensity values along the edge, showing how they vary from dark to light or vice versa. Subsequently, the LSF is derived by taking the derivative of the ESF. From this point forward, the analysis proceeds similarly to that of the crosshair pattern, culminating in the determination of MTF performance.

3.2.6 Distortion measurements

Even a small distortion may cause the image to look poor, but luckily the geometrical distortion of the waveguide can be corrected by pre-distorting the in-coupled image. The distortion of the waveguide can be analyzed using a dot pattern similar to the one described in ISO 17850:2015. The dot pattern is projected onto the waveguide and the

resulting image is acquired. However, this acquired image alone does not suffice to ascertain the distortion of the waveguide, as it incorporates the combined distortion effects of the projector lens and the camera lens. To obtain absolute distortion values, a reference image is essential. The dot pattern of the reference image is compared to the measurement image, and the difference between each dot location is calculated. The values can be used to calculate the relative distortion of each dot as

$$D = \frac{\theta - \theta_0}{\theta_0} 100\%, \tag{3.8}$$

where θ is the opening angle between the optical axis and the measurement image's dot location and the θ_0 is the opening angle between the optical axis and the reference image's dot location. By evaluating all the detected dot locations and the relative distances, a polynomial is fitted to these points. This polynomial can then be used to estimate the amount of distortion at any location of the field.

3.3 Current WG-IQ measurement system

The Waveguide Image Quality Measurement System (WG-IQ) developed by Optofidelity, as depicted in Fig. 3.8, serves as a precise and accurate tool for evaluating waveguides with diverse designs. The WG-IQ system employs a specialized camera lens, known as "OptoEye", which simulates the human eye, aligning with the objective of image quality measurement to assess visual perception from a human perspective. To attain sensor responses closely resembling the CIE XYZ tristimulus values, the camera can be equipped with specific color filters. Notably, the OptoEye is engineered to encompass a FOV of 80 x 60 degrees, catering to the requirements of large FOV waveguides.

The design of the WG-IQ system allows for measuring waveguides from both the eye side and the world side, making it a versatile tool. [54] This capability introduces a high level of complexity, yet it allows the system with adaptability to address various testing scenarios and waveguide configurations. As a result, the WG-IQ system offers comprehensive evaluation capabilities, catering to the diverse demands of optical engineers and manufacturers in the AR industry.

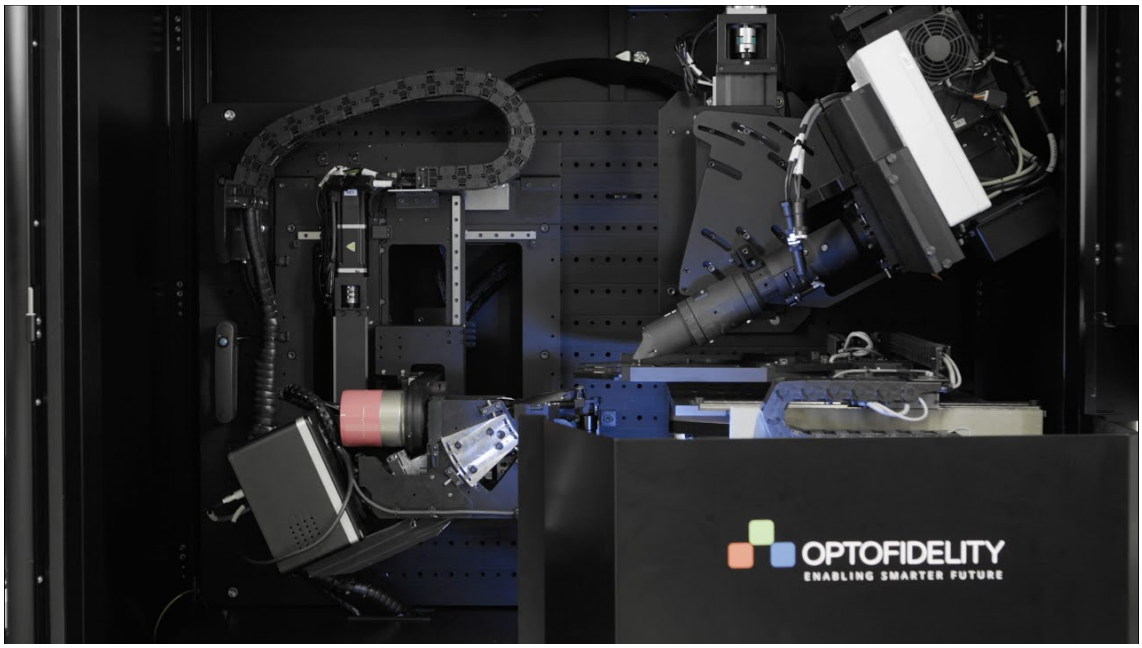

Figure 3.8. *Optofidelity's WG-IQ measurement system. [54]*

3.3.1 Accuracy of the system

The current design of the WG-IQ involves multiple dynamic components that require accurate alignments and calibrations to ensure optimal functionality and precision in the measurement process. To achieve this, an alignment method has been developed, allowing precise positioning of the camera, DUT, and projector at specific angles with accuracy at the level of tens of arcseconds. The alignment method relies on autocollimators, including the optical alignment of each instrument at any desired angle. These autocollimators work by projecting light onto the instrument and detecting the reflected light, enabling accurate angular alignment.

The standard WG-IQ configuration incorporates an alignment camera, utilized for aligning the DUT in both X and Y directions, while a confocal sensor serves to align the DUT's tilt. These alignments are executed by manipulating the hexapod, a highly accurate device capable of achieving translation accuracy up to 0.2 µm and angular accuracy better than 1 arcsecond.

In summary, the WG-IQ system's alignment and calibration procedures have been designed and implemented with high precision, ensuring the system's overall accuracy and reliability. By effectively aligning all components to the desired angles, the WG-IQ enables rigorous and reliable measurement of waveguides. The system's accuracy and reliability play a vital role in evaluating the optical performance and image quality of AR waveguides.

3.3.2 Measurement workflow

The WG-IQ measurement system can be configured to measure various different waveguide models with specific colors or patterns. However, the operator is required to define the model of the waveguide, providing crucial information such as the eye box position with respect to the in-coupler, desired wrap angle, and pantoscopic tilt. Once the DUT model is configured, the measurement recipe has to be generated. The measurement recipe contains critical parameters for conducting the measurements, including the power settings for each light-emitting diode (LED), the reticle pattern to be used, the desired analysis procedures, and the precise location of the eye box.

Importantly, the WG-IQ system supports the creation of multiple measurement recipes, allowing seamless switching between different measurement scenarios. Furthermore, operators have the option to configure and store multiple DUT models, enabling the evaluation of various waveguides as needed. Nevertheless, the operator is required to carefully select the appropriate DUT model and corresponding measurement recipe before starting the measurement.

The operational procedures of the WG-IQ measurement system are designed for simplicity and efficiency. The responsibilities of the operator primarily involve loading the DUTs into the DUT holder, placing the holder inside the tester, and closing the door. Then the operator selects the correct measurement recipe and DUT model and initiates the measurement process by pressing the start button. The whole workflow of WG-IQ is illustrated in Fig. 3.9. Upon starting the measurement, the doors are locked, the LEDs are activated and warmed up, and each instrument is moved to a home position in preparation for referencing.

The measurement sequence starts with referencing which means that the camera is pupil-matched with the projector which has roughly 3 mm eye relief. The camera captures images from each reticle pattern with each LED separately that are configured in the recipe. These images are called "reference images". After the reference images are taken, the LED channels are blocked and the camera moves to take dark frame images from the "dark pit", which is a black soft hole on the interior wall of the WG-IQ. The camera captures multiple dark frame images with different exposure times in order to estimate the noise of the camera with any exposure time. After dark current measurements, the DUT is loaded under the projector. The DUT is then identified by reading the bar code on it. The alignment camera detects the alignment marks on the DUT and aligns the DUT so that the exit pupil of the projector matches the input pupil of the waveguide precisely.

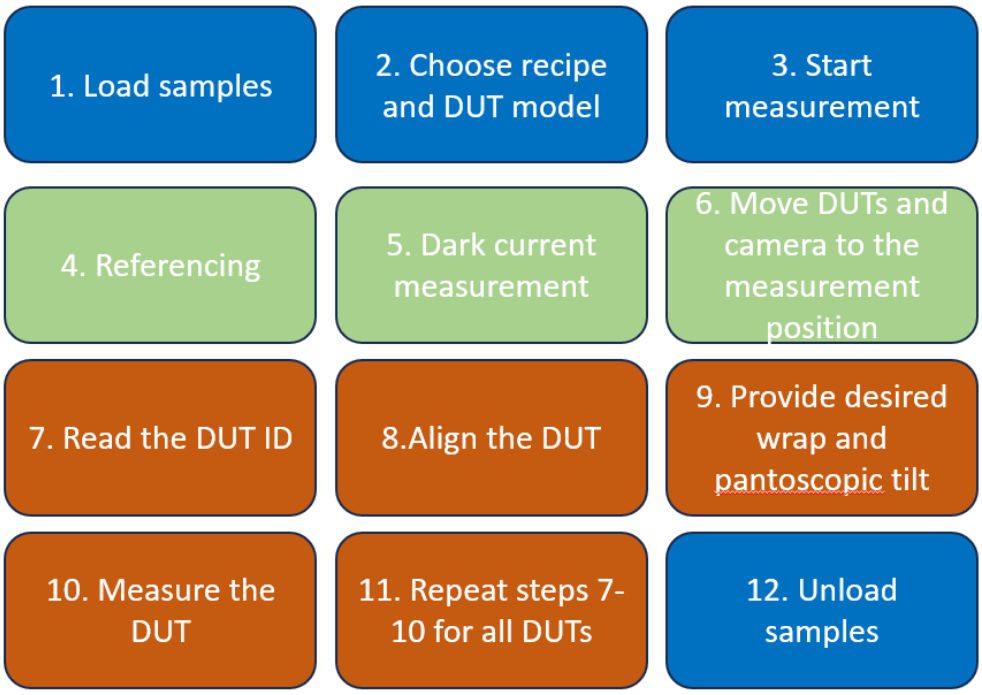

Figure 3.9. *Measurement workflow. Operator-related steps are marked as blue, calibration and referencing-related steps are marked as green, and DUT-specific things are marked as orange.*

After the alignment, the DUT is tilted to the designed pantoscopic tilt and wrap angle using the hexapod whose pivot point is defined to be exactly at the exit pupil of the projector. The camera moves to the measurement position according to the DUT model and the desired reticle patterns are projected into the waveguide and the transmitted image is captured by the camera. The measurement follows the measurement recipe and runs the predefined analysis in the background. After all DUTs are measured, they are unloaded, the doors are unlocked and results are saved at the desired location. At this point, the operator may change the DUTs on the loader and start a new measurement.

3.3.3 Challenges of waveguide testing

The continuous development of the AR industry and the evolving nature of waveguide designs require a measurement system that can accommodate both current and future waveguide models with varying properties and requirements. The WG-IQ measurement system is specifically designed to address these ever-changing demands, offering the desired flexibility. However, this adaptability comes at the cost of increased complexity and higher expenses, making the system less suitable for mass production scenarios, where waveguide designs remain consistent and throughput has to be high. Additionally, the presence of multiple moving axes in the system can lead to reduced overall accuracy.

Several key challenges arise in waveguide measurements. Firstly, the flexibility require-

ments pose a significant challenge. The tester must be capable of measuring waveguides from both the eye side and the world side, depending on the specific waveguide design, necessitating a flexible setup with at least four degrees of freedom. Secondly, capturing a reference image with eye-side waveguides presents a major challenge. To obtain an accurate reference image, precise pupil-matching between the camera and projector is essential. While the WG-IQ system achieves high accuracy in axis alignment and demonstrates high repeatability in linear and angular movements, these advantages come at the expense of substantial costs and extended lead times.

The establishment of pupil match is currently achieved by aligning the camera and projector with each other, ensuring their pupils are matched. This alignment has to be very accurate, as even a minor misalignment can lead to vignetting in the reference image, directly affecting certain analysis outcomes. Precise alignment is crucial to avoid deviations and alterations in the obtained results. Thus, achieving accurate alignment between the camera and projector pupils becomes imperative.

Following the capture of reference images, the camera is subsequently moved to the measurement location. For waveguides operating in reflection mode, this means a 180-degree rotation of the camera to face the eye side. In contrast, for transmission mode waveguides, rotation of the camera is not necessary. This movement is illustrated in Fig. 3.10.

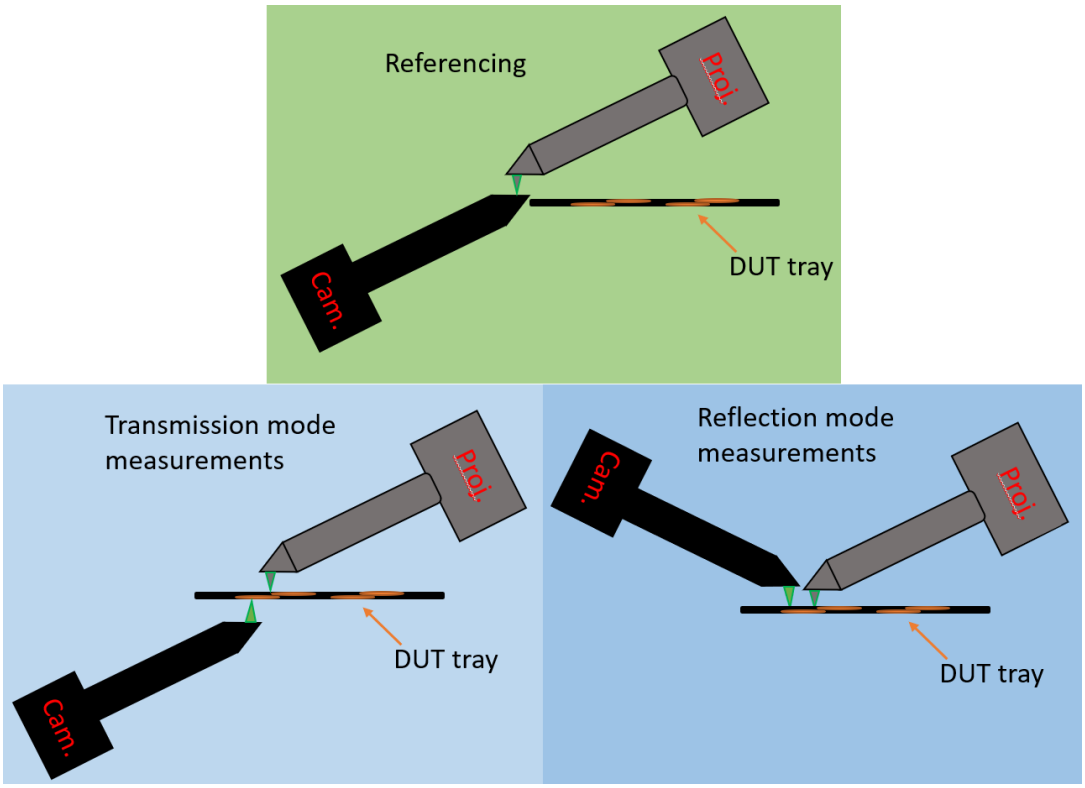

Figure 3.10. *Illustration of reference measurement, transmission mode measurement and reflection mode measurement.*

While movement in translation space is essential to facilitate measurements at different eye box locations, rotational movements can be minimized or avoided altogether. In this thesis, the objective is to explore and refine an advanced method to eliminate angular movement from the system while still satisfying the stringent requirements of a high-accuracy measurement setup. By developing this new approach, we aim to enhance the precision and robustness of the measurement system, ensuring reliable waveguide evaluations. Through the implementation of this innovative technique, we aspire to optimize the alignment process and reduce complexities and costs.

3.3.4 Improvements of testing procedure

The challenge presented by the use of mirrors lies in handling pupil mismatch: How can we obtain an unvignetted reference image if the camera and projector are not precisely pupil-matched? Additionally, the implementation of mirrors may impose limitations on the maximum FOV. To address these challenges, we propose a solution known as "field reconstruction." This innovative method involves capturing multiple vignetted images at different locations on a plane and subsequently combining them into a single, unvignetted image. With this field reconstruction method, we aim to overcome the limitations posed by pupil mismatch and mirror usage. More on this in Chapter 5.

In this thesis, we are developing a novel method to capture the reference image without relying on pupil match, enabling seamless operation with reflection mode waveguides without the need to rotate the camera. As the reference image is an essential component of waveguide measurements, it is crucial to ensure that any potential pupil mismatch does not introduce unwanted aberrations or vignetting. To minimize aberrations, the use of additional lenses, such as relay lenses, is impractical, as they can introduce distortion. Instead, we explore an alternative solution that includes employing flat mirrors.

In an ideal scenario, flat mirrors do not induce optical aberrations, as light rays strictly obey the law of reflection. However, consumer-grade mirrors may not possess perfectly flat surfaces, leading to deviations and distortions in the reflected image. To mitigate this issue, very flat mirrors can be used, such as $\lambda/20$ mirrors, which feature highly smooth, validated surfaces.

4. PUPIL MISMATCH EXPERIMENT

In this experimental study, an imaging system, called "Nautilus", was used. It is primarily employed for evaluating the MTF performance of waveguides. However, in this experiment, the system was repurposed to detect the impact of pupil mismatch and the implementation of a dual-mirror setup on the MTF performance of the lens. In the initial phase of the experiment, reference images were obtained by using various combinations of wavelengths and aperture sizes. Subsequently, the images were captured through the dual-mirror configuration, using the same combinations of wavelengths and aperture sizes. With the acquired image data, the MTF values were calculated to quantify the lens performance under the influence of pupil mismatch and dual-mirror utilization. The resulting MTF data were then used to construct MTF graphs, providing visual representations of the lens performance. By using the "Nautilus" imaging system in this unconventional way, insights into the effects of pupil mismatch and dual-mirror implementation on the lens's MTF performance were gained.

4.1 Experimental setup

The experimental setup consists of a dual mirror, projector, and camera that are designed to ensure diffraction-limited performance at pupil match. The configuration of the setup is shown in Fig. 4.1. To achieve infinity focus for both the camera and projector, a commercially available autocollimator was used. The infinity focus was first achieved for the camera using the autocollimator. Subsequently, the focus of the projector was adjusted to infinity by fine-tuning the focus until the projected image appeared sharp on the camera. The projector had a crosshair reticle pattern with a line width of 10 µm, that was used to align the system in angular space. The camera's FOV was approximately 3 degrees.

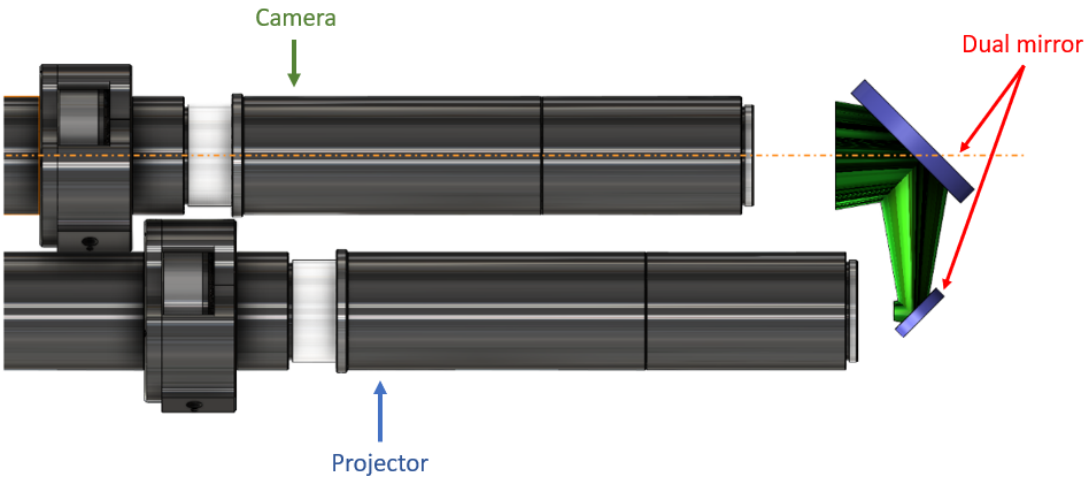

(a) *3D model of the setup*

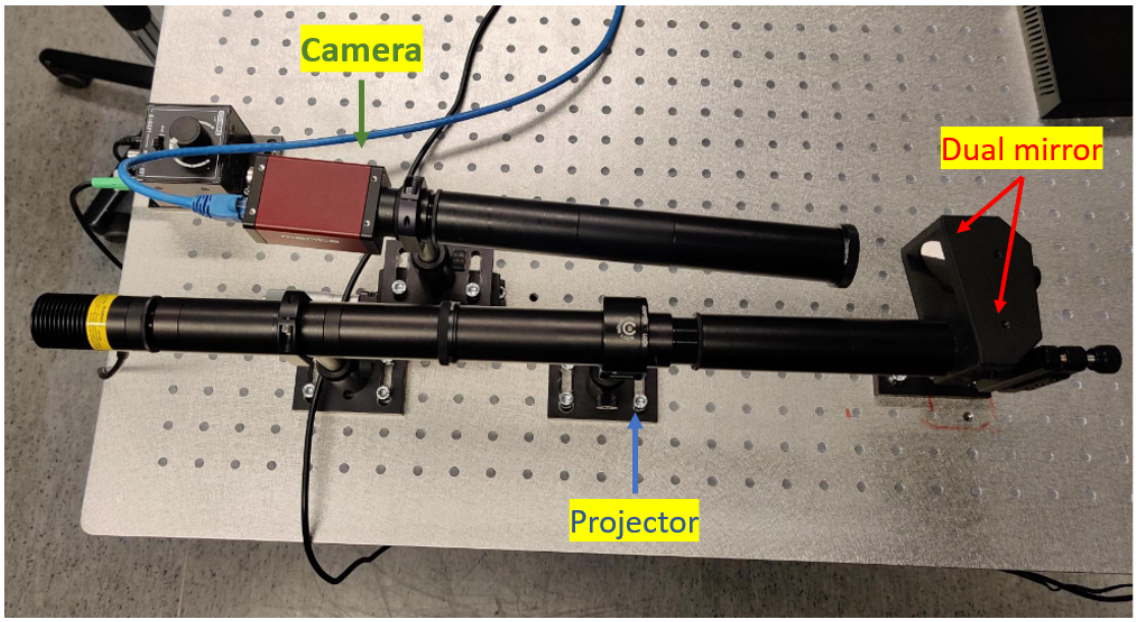

(b) *Actual implementation of the setup*

Figure 4.1. *(a) Ideal design for the "Nautilus" setup (b) The actual setup.*

The dual mirror included two mirrors with diameters of 15 mm and 40 mm. Both of the mirrors have surface flatness of $\frac{\lambda}{20}$. With such a high flatness the surface roughness effects on the MTF values could be minimized. This guaranteed that the mirrors were working as ideally as they could and consequently, did not affect the MTF values. This enabled to better evaluate the pupil mismatch's effects on the MTF values.

The dual-mirror holder, shown in Fig. 4.2, was designed to be used also in the field scanning experiment so that the beam could expand and still the second mirror would be larger than the beam diameter when it hits it.

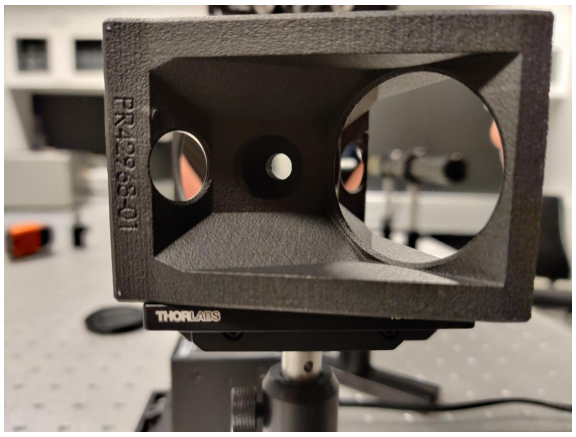

Figure 4.2. *The mirror holder.*

The experimental setup contains an angle of 90 degrees between the two mirrors, ensuring that the ideal ray incident on the first mirror will be parallel to the reflected beam from the second mirror. However, during our experimentation, it was observed that the actual angle between the mirrors deviated slightly, measuring approximately 91.5 degrees, primarily attributed to 3D printing tolerances. Nonetheless, it is important to note that this slight variation in the angle between the mirrors does not significantly impact the measurement results, provided all incident light rays fully reflect from the mirrors.

4.2 Measurements and Results

The projector was placed on the optical table and locked in place. That was used as the reference for the alignment of the other components. Next, the camera was placed such that it was pupil-matched with the projector which is shown in Fig. 4.3.

Figure 4.3. *The reference position with pupil match.*

After the alignment, the crosshair reticle was rotated as close as possible to a 0-degree angle in the camera's image. This was done by monitoring the camera image and rotating

the physical reticle inside the projector. Python-based software was employed to show the angle of the reticle in real time. The user interface of the software is shown in Fig. 4.4.

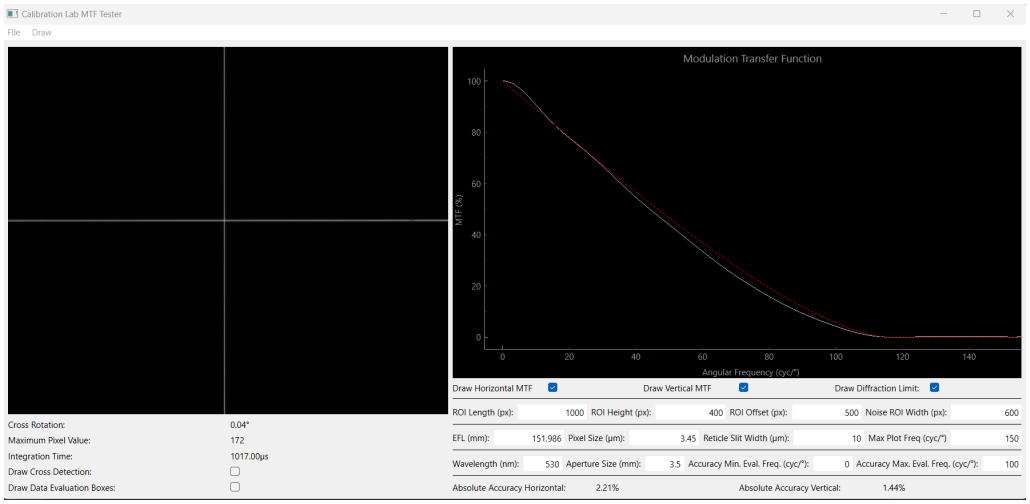

Figure 4.4. *The Python-based software shows the crosshair orientation and MTF graph with theoretical diffraction limit.*

During all measurements, a 6.0 mm aperture was used for the projector as the limiting aperture was desired to be the camera's aperture. The projector was not touched after its aperture was set and the reticle aligned.

The idea of this experiment was to show that the dual-mirror, and consequently pupil mismatch, is not causing any unwanted effects on the MTF values. In this experiment, specific wavelengths were employed for each color, red, green, and blue, which were respectively set at 625 nm, 530 nm, and 455 nm. Additionally, the measurements were repeated using aperture sizes commonly found in AR waveguides, mirroring the dimensions of human pupils in both well-illuminated and low-light environments. The chosen camera aperture diameters were 2.50 mm, 3.50 mm, and 5.00 mm.

The measurement was started by capturing the reference images from the pupil match situation shown in Fig. 4.3. Next, the images were captured through the dual mirror with the setup shown in Fig. 4.1. The MTF was calculated from the crosshair pattern of each image by averaging the MTF values of all arms of the crosshair. The resulting MTF graphs for all wavelengths are shown in Fig. 4.5. The MTF measurements for red wavelength failed due to poor LED alignment.

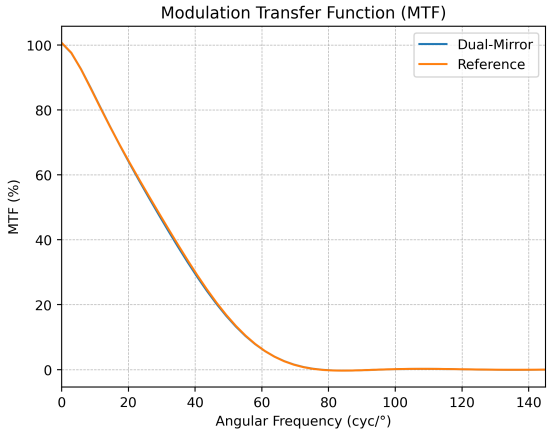

(a) *Blue (455 nm), 2.5mm aperture.*

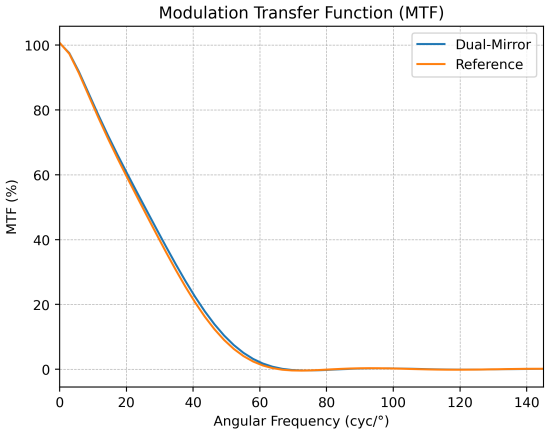

(b) *Green (530 nm), 2.5mm aperture.*

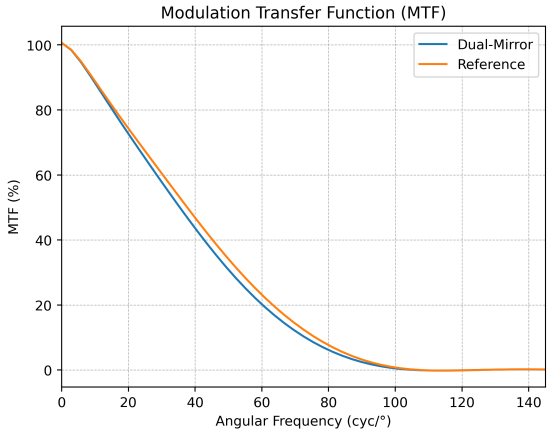

(c) *Blue (455 nm), 3.5mm aperture.*

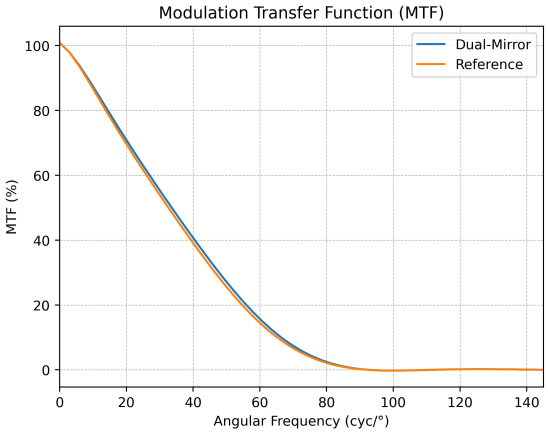

(d) *Green (530 nm), 3.5mm aperture.*

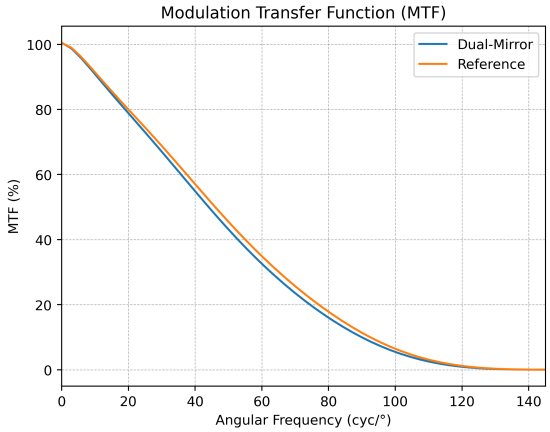

(e) *Blue (455 nm), 5.0mm aperture.*

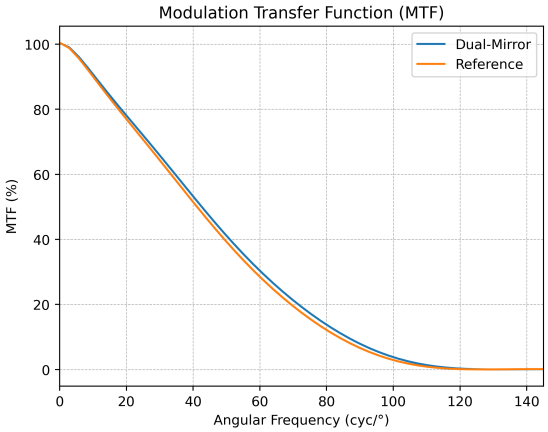

(f) *Green (530 nm), 5.0mm aperture.*

Figure 4.5. *(a-f) MTF graphs comparing reference images' and measurement images' MTF values.*

Based on the measurement results, some minor inconsistencies were noticed between the measurements. These discrepancies arise due to the challenging nature of adjusting the aperture size precisely. The aperture sizes were adjusted with the accuracy of 0.1 mm which may lead directly to small deviations in the results.

Furthermore, a detailed analysis of the MTF curves acquired using the two-mirror setup and the reference images shows notable similarities. Consequently, it can be concluded that the presence of mirrors in the system does not lead to a decrease in the MTF performance. Also, during the measurements, it was observed that the imperfect pupil match had a negligible impact on the MTF curve. Specifically, even when the camera's pupil was shifted within a range of ± 10 mm from the projector, no noticeable variations were observed in the MTF curves. As a result, the referencing process can be conducted effectively, even in the presence of pupil mismatch. This implies that referencing should be possible with field reconstruction.

5. PUPIL SCANNING EXPERIMENT

In this chapter, the concept and implementation of field reconstruction are described. The pupil scanning setup was developed and built as a proof-of-concept (POC) for field reconstruction. The primary objective of this experiment is to establish field reconstruction, particularly in scenarios characterized by significant pupil mismatch, while maintaining a feasible 2 percent tolerance. As discussed in subsection 3.3, performing referencing without pupil match would enable to design simpler and more efficient optical systems.

5.1 Experimental setup

The experimental setup which is used for the POC of field reconstruction, illustrated in Fig. 5.1, is assembled on an optical table. The key components of the setup contain the camera, projector, dual mirror, and hexapod, each playing a critical role in the successful implementation of the field reconstruction. Additional components, including the autocollimators and the tracking mirror, are also integrated within the setup, fulfilling the essential need to monitor the angular movement of instruments.

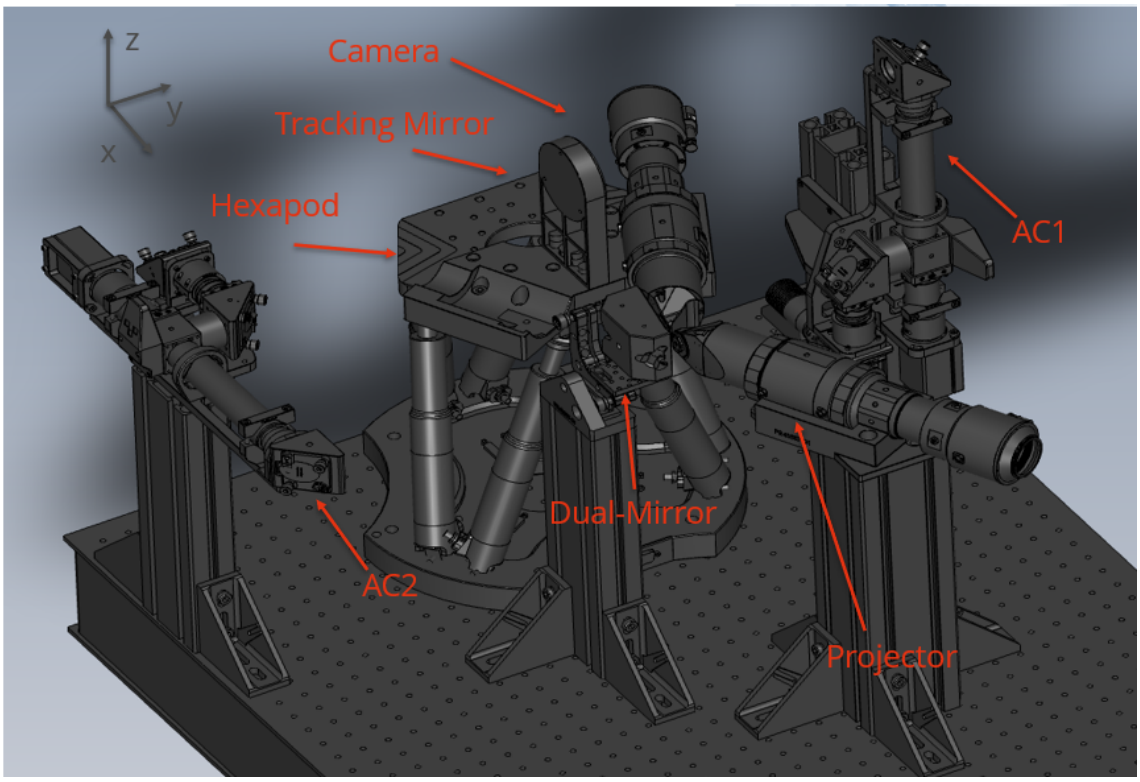

Figure 5.1. *Schematic image of the field reconstruction POC setup.*

As the aim of this POC is to prove the feasibility of field reconstruction as an effective alternative for referencing in imaging, high precision, and traceability are required. Given that the camera captures images at distinct spatial locations, it is imperative to ensure the accuracy and traceability of the camera's movement. The coordinates of the hexapod must be documented for each image acquisition. These spatial coordinates serve as vital input data for the image combination algorithm, which is described in greater detail in subsection 5.3.

5.1.1 Camera, projector, and dual-mirror

The camera utilized in this study comprises the Allied Vision Prosilica GT 6400 camera sensor integrated with Optofidelity's OptoEye lens. The camera sensor has a pixel size of 3.45 µm x 3.45 µm. The OptoEye lens is securely attached to the camera sensor using an F-mount and is precisely focused to infinity using a commercial autocollimator. The camera boasts an impressive FOV spanning 80 x 60 degrees, with a theoretical angular resolution of 73.0 pixels per degree. Furthermore, the OptoEye lens has a 3.0 mm entrance pupil, making it an ideal choice for evaluating the viability of field reconstruction as a referencing method for future measurement systems.

The projector's light engine was originally designed to measure the checkerboard contrast of the OptoEye lens. The light engine incorporates the Thorlabs M530L4 LED as its light

source, boasting a wavelength of 530 nm and a full width at half maximum of 35 nm. The light engine has an interchangeable reticle that can be used to evaluate different properties of the system. For instance, the non-symmetric crosshair pattern, depicted in Fig. 5.2, can be used to evaluate the impact of field reconstruction on MTF values, while the solid reticle pattern could be used to test potential deviations in uniformity or efficiency within the system. Although these measurements will be important, they are outside the scope of this thesis.

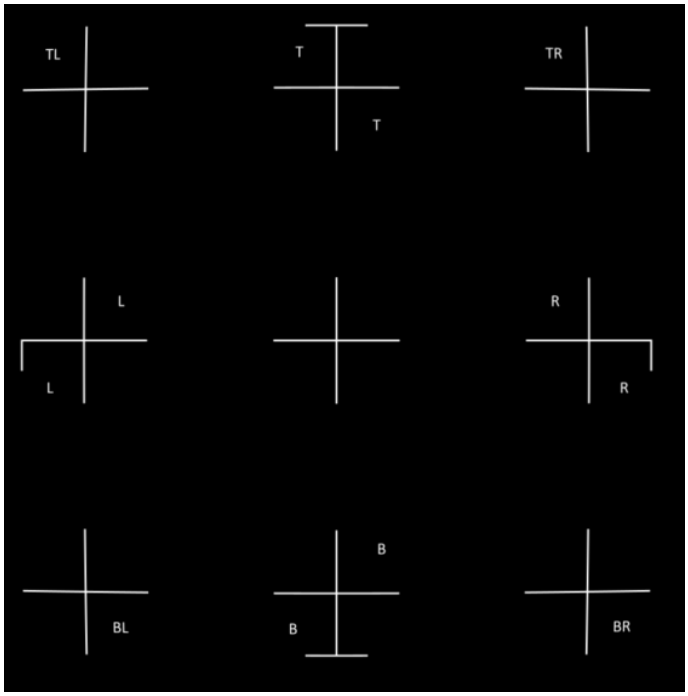

Figure 5.2. *The design of the MTF crosshair reticle pattern.*

The light engine is completed by adding another OptoEye to it and the exit pupil is adjusted to roughly 3.0 mm diameter. Achieving proper focusing of the projector involves aligning the camera's and projector's pupils through pupil matching, followed by focus adjustments until the projected image attains optimal sharpness. The dual mirror is the same as the one utilized in the Nautilus experiments. However, in this configuration, the dual mirror imposes certain restrictions on the maximum FOV. This constraint arises due to the phenomenon of pupil expansion, illustrated in Fig. 5.3. Consequently, the maximum FOV achievable with this setup was tested to be 23 x 23 degrees, which, in turn, limited the reticle size to 20 x 20 degrees.

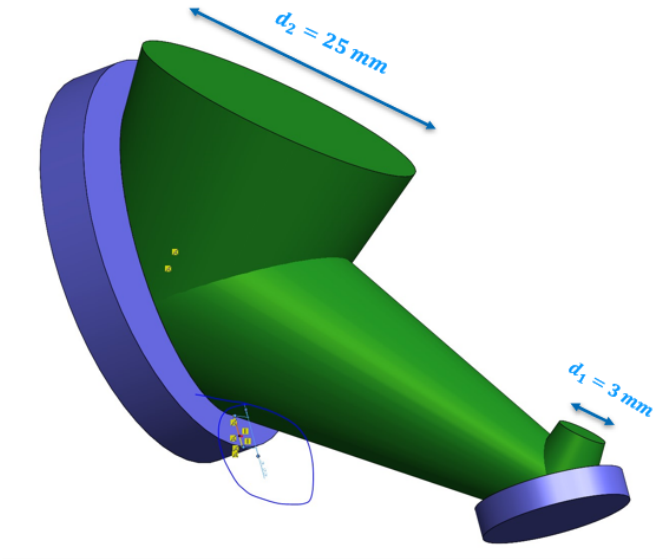

Figure 5.3. *The expansion of the pupil.*

5.1.2 Angular movement monitoring with autocollimator and tracking mirror

The autocollimator is used to monitor the angular movement of the hexapod. This monitoring becomes crucial, as any unidentified angular movement in the camera's position could lead to the failure of the field reconstruction. To ensure accurate measurements, the angular movement is continuously tracked and monitored with the autocollimator and tracking mirror. The underlying concept involves obtaining precise knowledge of the angular error at each measurement location, which allows for necessary corrections in the captured images if required.

Any angular movement less than 30 arcseconds, equivalent to roughly 30 pixels, goes undetected by the OptoEye due to its limited angular resolution. However, image correction becomes necessary when the angular movement exceeds 1 arcminute because the image shifts by at least one pixel length on the camera sensor. Such correction can be achieved through image processing techniques, but careful consideration of the image processing steps is essential. Notably, the flatfield correction must be performed prior to the shifting process, as it has varying effects on individual pixel locations.

The alignment process of the autocollimator involves two steps. Starting with the alignment of the camera in the correct angular position concerning the dual mirror and projector. Once the camera is precisely aligned, the autocollimator can then be aligned to the tracking mirror. A preliminary alignment of the autocollimator to the center of the autocollimator camera sensor is performed, and the resulting camera image is depicted in Fig. 5.4. Throughout the measurements, the maximum detected angular error was observed to be 25 arcseconds, indicating that image shifting was not necessitated.

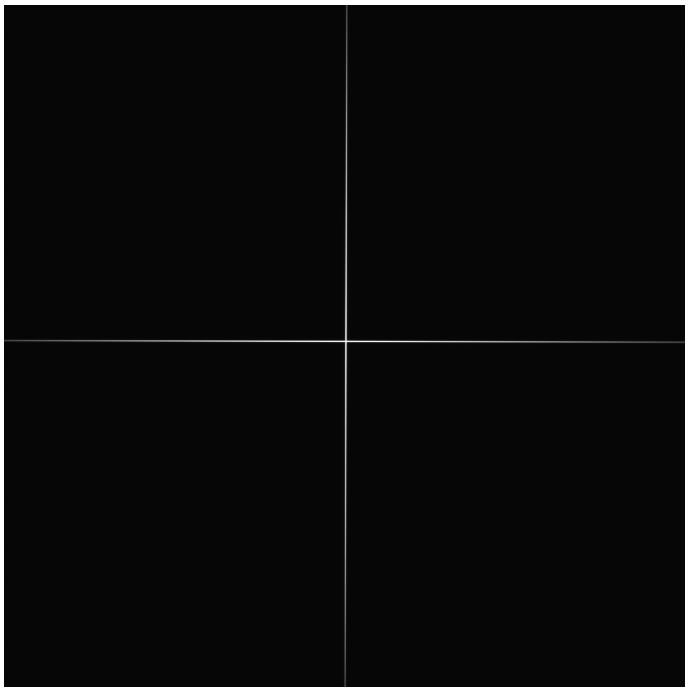

Figure 5.4. *Example of autocollimator image.*

The second autocollimator, denoted as "AC2" in Fig. 5.1, served the purpose of investigating the possibility of aligning the optical axes of both the camera and projector to be parallel. To achieve this alignment, the projector was fixed in position, and the autocollimator was initially aligned to the projector lens in a manner that allowed the reflected beam to coincide with the internal cross of the autocollimator. This alignment ensured that the optical axis of the autocollimator matched that of the projector.

Next, the camera was positioned in front of the projector, facing the autocollimator. The hexapod was then utilized to rotate the camera until its optical axis matched that of the autocollimator. Upon successful alignment, the camera was moved back to its original position, and the angular movement was monitored using the first autocollimator and tracking mirror. After moving the camera back next to the projector, the optical axis would be parallel between the camera and the projector.

This alignment process may hold significant importance, as it could be used for potentially aligning the two instruments at specific angles in future applications. The successful alignment demonstrated that the autocollimators could be effectively utilized for precise alignment of the camera and projector's optical axes.

5.2 Pupil scan experiment and details

The main goal of this experimental study is to validate the feasibility of obtaining information equivalent to that obtained through pupil match referencing, using the field reconstruction method with multiple vignetted images. The OptoEye lens has an optimal

eye relief of approximately 3.0 mm. During the reference measurement, the system is pupil-matched, ensuring that the camera is positioned at a 3.0 mm eye relief. The reference image, depicted in Fig. 5.5, shows the results obtained from the pupil-matched configuration.

It is essential to acknowledge that all measurement images presented in this chapter have been cropped to a rough FOV of approximately 20.5 x 20.5 degrees. This cropping is performed to exclude the dark regions outside this specified FOV, as they are not relevant to the objectives of this experiment and do not contribute to the analysis and evaluation of the field reconstruction method. The cropped images provide a clear and focused representation of the relevant data and are sufficient for the purposes of this study.

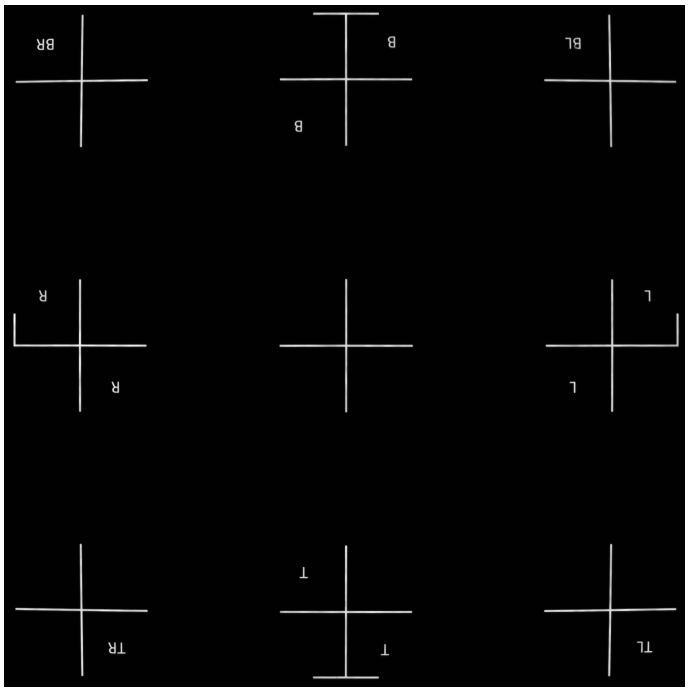

Figure 5.5. *Reference image.*

In this experiment, the use of a dual mirror introduces an increased working distance of approximately 67 mm, resulting in a significant expansion of the exit pupil diameter from 3 mm to 25 mm, as illustrated in Fig. 5.3. This expansion of the pupil leads to highly vignetted images, where only a small part of the field is visible. The FOV of the partially vignetted area seen in the image can be calculated with

$$\mathrm{FOV} = 2\arctan(\frac{d_{\mathrm{exp}} + d_{\mathrm{ep}}}{2L}), \tag{5.1}$$

where d_{exp} is the diameter of the exit pupil, d_{ep} is the diameter of the entrance pupil and L is the distance between the pupils. Equation 5.1 can be used to estimate the visible FOV of the pupil which is plotted in Fig. 5.6.

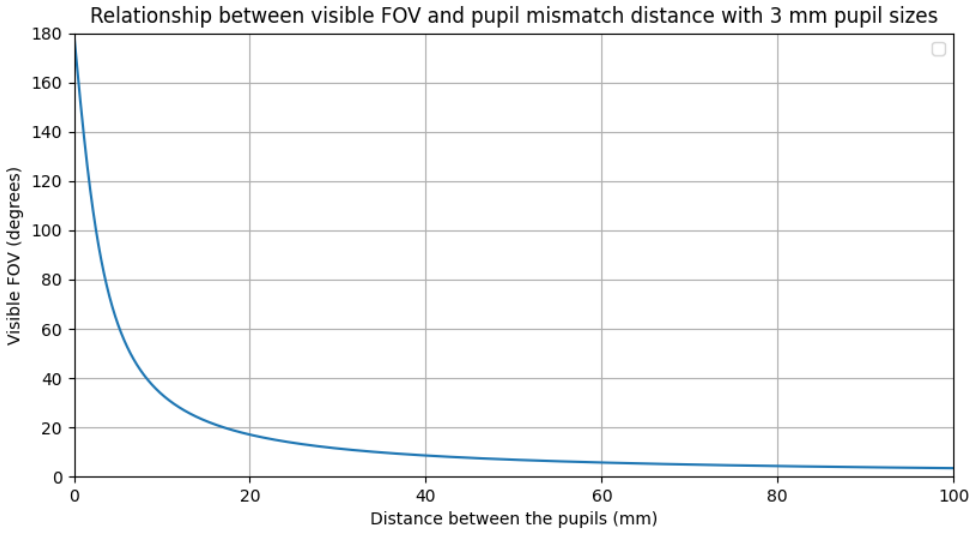

Figure 5.6. *Visible FOV for 3 mm exit and entrance pupils.*

To overcome the vignetting issue, pupil scanning can be used. This involves moving the hexapod in the xz-plane, causing the camera to move in small steps to cover the entire pupil area. An image is captured after each step, enabling the visualization of different parts of the field and facilitating the imaging of the entire field. Figure 5.7 illustrates the results of this pupil scanning process, showing nine separate images taken at different positions in the xz-plane.

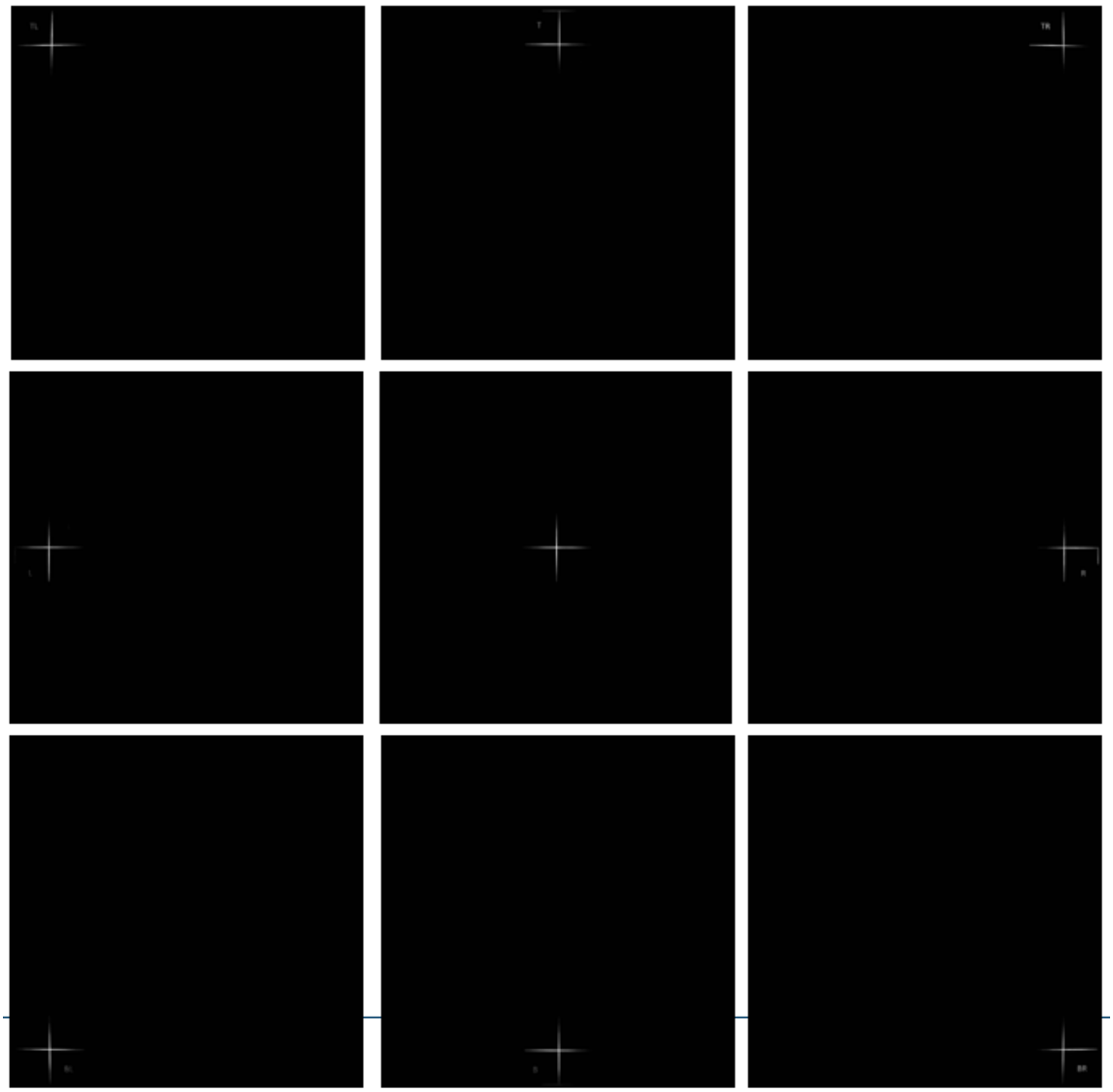

Figure 5.7. *There are 9 separate vignetted images next to each other. The location of each image is 9 mm away from each other.*

The step size used in the pupil scan is constrained by the distance between the entrance and exit pupils and the size of their pupils, as indicated in Eq. 5.1. However, even at a distance of 67 mm, the visible FOV remains roughly 4-5 degrees, suggesting that the pupil scan can be performed for a larger FOV, such as 20 x 20 degrees, using only 25 images. Despite this advantage, the challenge lies in the fact that these images are still partially vignetted.

Fortunately, it is observed that the centers of the partially vignetted areas exhibit minimal vignetting, accounting for approximately 5 % of the visible FOV. This region can be considered "non-vignetted" for the human eye as the vignetting effect is negligible in this area. Note that this 5 % approximation is only valid for visual detection, and this would not be sufficient for high-accuracy referencing. For referencing purposes, the non-vignetted area is analyzed to be roughly 3 %. In general, the smaller the step size the more accurate

the field reconstruction is. Regardless of this, the pupil scan can be accomplished with a finite number of steps. In the case of a 20 x 20-degree reticle, a total of at least 10000 steps would be required. These small steps ensure that each part of the field is imaged without noticeable vignetting, ensuring high-accuracy field reconstruction. However, note that this approach is time-consuming due to the large number of steps involved.

The vignetting is not well illustrated with the crosshair pattern so the solid reticle is used to demonstrate the effect of the different step sizes. The reference image which is acquired with pupil match is shown in Fig. 5.8. There is some dirt on the reticle on purpose which can be seen in the reference image as stains. Those stains were used to analyze whether impurities have some effect on the field reconstruction algorithm. The combined images with different step sizes are illustrated in Fig. 5.10.

Figure 5.8. *Image of the solid reticle reference.*

5.3 Field reconstruction methods and results

In this thesis, two different methods were studied to perform the field reconstruction. Both of the methods involve using a small step size to utilize only the non-vignetted parts of each image. These methods include a combination using the maximum pixel value and a combination of non-vignetted areas from each image.

5.3.1 Maximum pixel value method

The first field reconstruction method presents a straightforward and computationally efficient approach to field reconstruction. It relies on the fact that the non-vignetted pixels have larger pixel intensity than the partially vignetted areas in other images. The principle underlying this method is simple. The images are stacked together, and for each

pixel, a comparison is made to retain only the pixel with the maximum value across all images. This algorithm is quite similar to the well-known technique called "multi-exposure HDR capture" [55]. Although the algorithm for combining the images is similar, the image acquisition is different as it uses different exposure time for each image.

Consequently, there is no need to consider where the non-vignetted pixels are located in a specific image, and no additional calculations are required. However, the main drawback of this method is that it can amplify noise in the image. Since it preserves the maximum noise value for each pixel, particularly in darker regions, the noise can impact the accuracy and quality of the reconstructed image. Figure 5.9 shows the field reconstructed image with the maximum pixel value method.

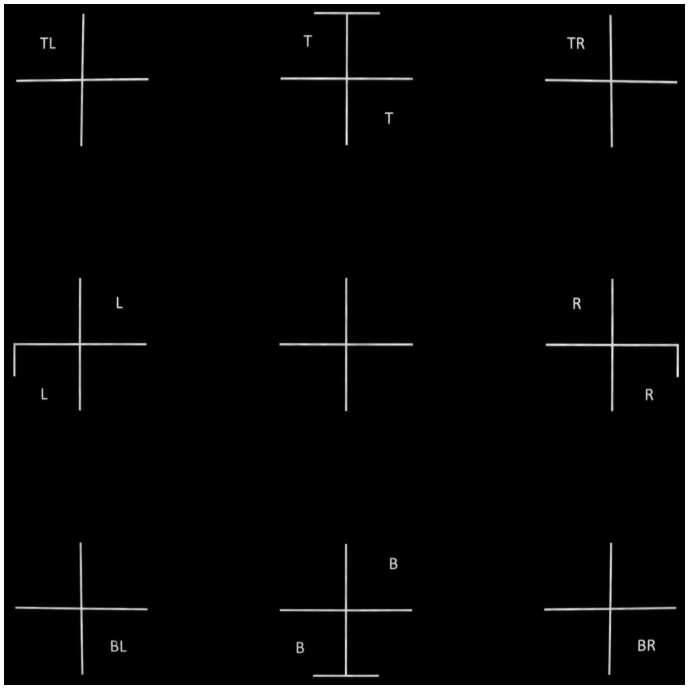

Figure 5.9. *Field reconstructed image with 0.5 mm step size.*

By comparing the reference and measurement images, it can be noticed that the image is rotated 180 degrees. This means that comparing the reference and the field reconstructed images requires some image processing such as rotating and shifting the image. Shifting is a consequence of the reticle alignment as the reticle is not aligned to the center of the camera sensor but to the optical axis of the camera lens which is verified with an autocollimator.

The effect of the different step sizes is demonstrated in Fig. 5.10. Basically each visible "rectangle" is one image that has been used to perform field reconstruction with maximum pixel value. There is no vignetting visible with 0.25 mm step sizes which indicates that the step size is sufficient for referencing.

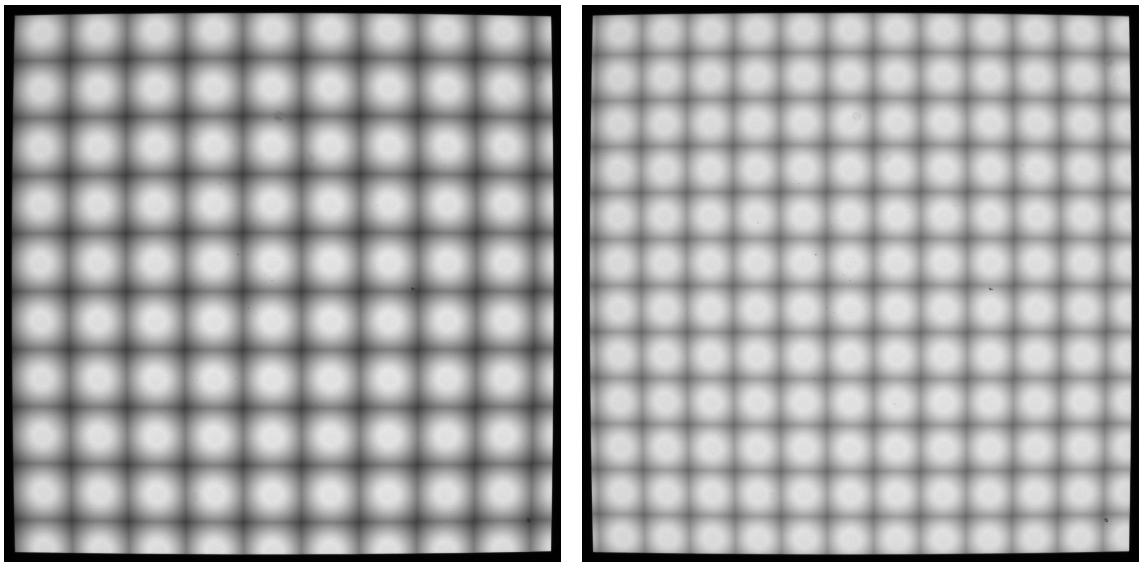

(a) *Solid reticle with 2.5mm step size.*

(b) *Solid reticle with 2.0mm step size.*

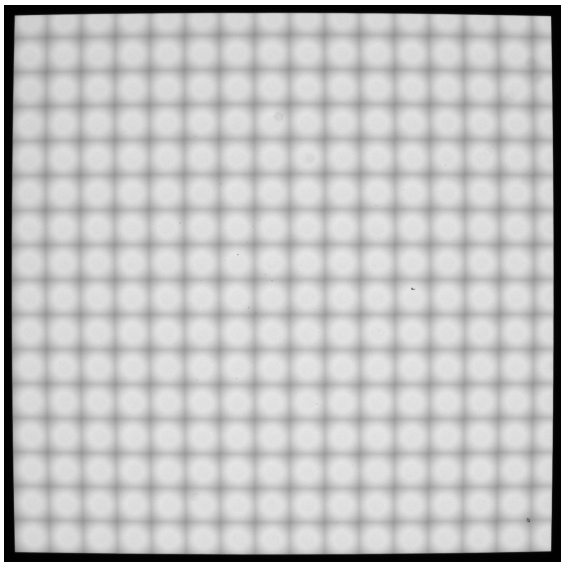

(c) *Solid reticle with 1.5mm step size.*

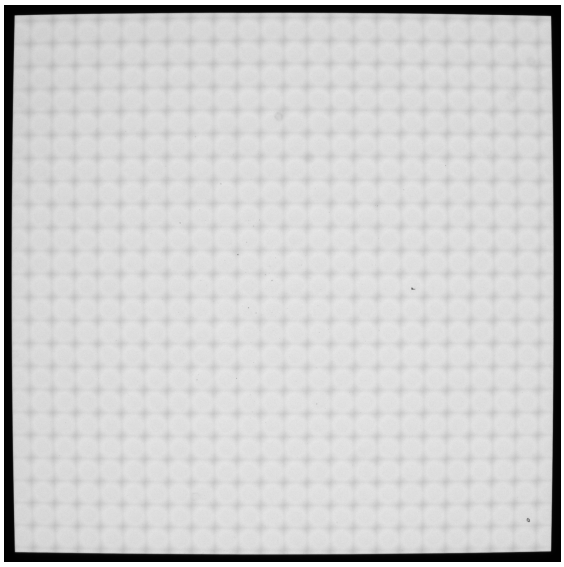

(d) *Solid reticle with 1.0mm step size.*

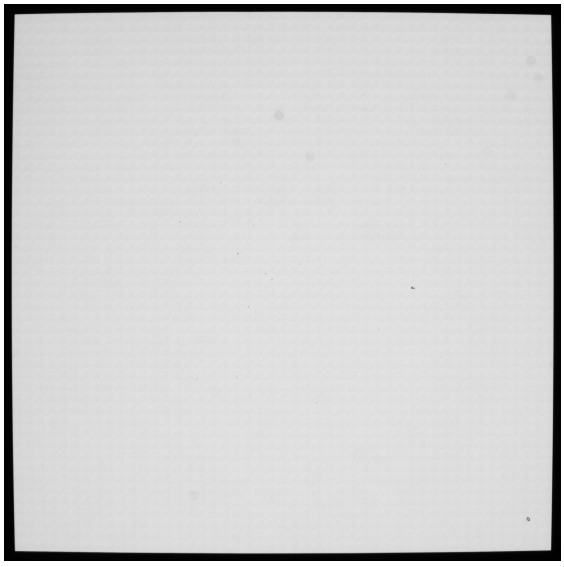

(e) *Solid reticle with 0.5mm step size.*

(f) *Solid reticle with 0.25mm step size.*

Figure 5.10. *(a-f) The effect of different step sizes on field reconstruction. The mismatch between the pupils is 67 mm. The maximum pixel value method was used to form these images.*

Ultimately, the goal is to compare the reference image and the field reconstructed image and analyze the difference between them so the rotating and shifting of the image are necessitated. Rotating an image 180 degrees can be done by flipping the image first in the horizontal direction and then in the vertical direction. This can be done in most image processing software automatically.

The shifting of the pixels can be done by moving each pixel row up or down and each pixel column right or left. As this deletes some pixels on the edges as they go outside of the image, pixels with a value of 0 can be added to the opposite edges to keep the image the same size. If the FOV of the reticle pattern is not close to the edges, this kind of shifting can be done without manipulating the information of the image.

5.3.2 Field location method

The second method requires the coordinate information of each image. It calculates the pixel coordinates for the non-vignetted area using the robot coordinates at that specific location where the image was captured. Basically, it uses the physical distance in the x and y directions between the reference coordinates and the robot coordinates where each image was captured. The reference coordinate is the robot coordinate where the center of the reticle or the zero-degree field angle is non-vignetted. Next, both the azimuth and elevation angle are calculated according to the robot coordinates. This is illustrated in Fig. 5.11.

The calculated angles are translated to pixels by multiplying them by the angular resolution of the camera which is 73 pixels per degree for OptoEye. This will give the pixel location for the non-vignetted area for each image without analyzing each image separately. During this study, it was assumed that the angular resolution of the camera to remain constant across the camera sensor because only a very small FOV was used.

However, this method necessitates accurate robot coordinates to be saved for each image and careful measurement of the distance between the pupils. If either of these is not accurately measured, the outcome will have visible marks that are caused by choosing the wrong part of each image. This is due to the tangential function

$$\alpha = arctan(\frac{L}{PD}), \tag{5.2}$$

where L is the distance between the current robot coordinate and the coordinate at the middle of the reticle and the PD is the distance between entrance and exit pupils. Figure 5.11 illustrates that the visible part of the reticle in the image is not linearly related to the robot coordinates.

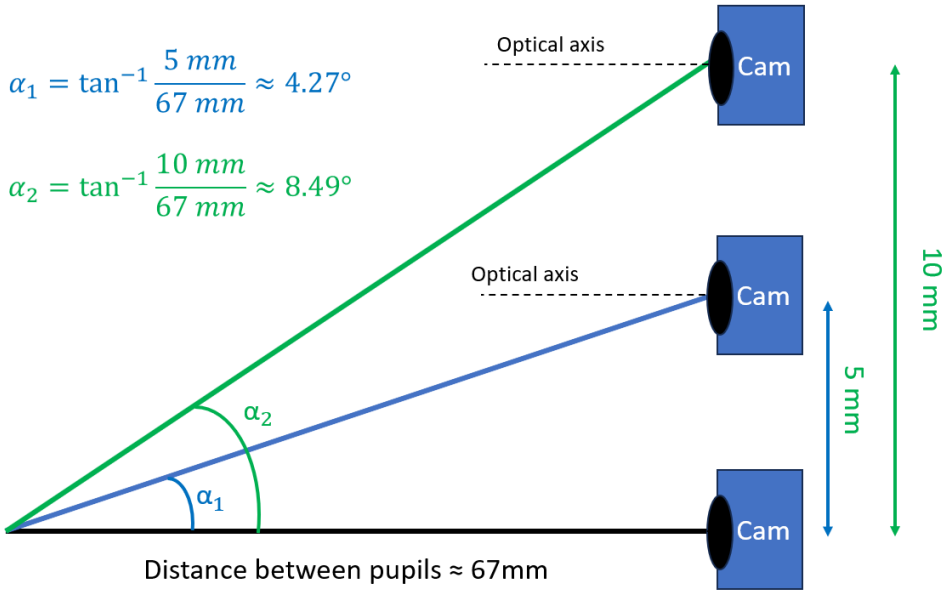

Figure 5.11. *The field angle of the visible part of the reticle in the camera sensor.*

The field reconstructed image with the field location method is shown in Fig. 5.12.

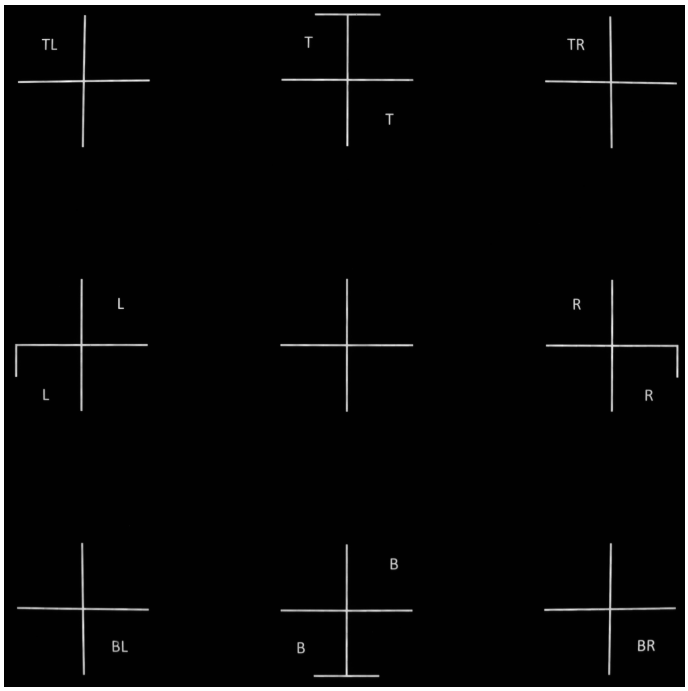

Figure 5.12. *Combination of the non-vignetted areas for crosshair pattern.*

There are no visible differences between Fig. 5.12 and Fig. 5.9. However, there are slight differences between the dark regions in the image that might affect for example the contrast or MTF values. The average pixel value of the dark regions with the maximum pixel value method after dark frame subtraction is 3.6, but only 1.3 with the field location method. This indicates that there is more noise with the maximum pixel value method

compared to the field location method. This information is very useful as it can be used to potentially compensate for the noise in the images in the future.

5.4 Future improvements and applications

The results presented suggest that field reconstruction is a viable approach, but the image-combining algorithm needs further development to expedite processing. Currently, the process entails capturing full-resolution images at each robot coordinate location, resulting in the acquisition of over 10,000 images each time. However, this approach is impractical for real-world measurement systems due to memory limitations. Fortunately, ongoing efforts are focused on avoiding the need to store 10,000 full-resolution images.

Two distinct approaches are currently being explored to address this challenge. In the first approach, each image is immediately combined, and the raw data is deleted, reducing the storage requirement to just one image. However, this approach raises concerns about traceability, as deleting the original data can make it challenging to verify the results. Nonetheless, this method aligns well with the maximum pixel value approach.

The second approach involves cropping each image to retain only the visible vignetted area, significantly reducing the storage space required for each image. This approach also permits the preservation of raw data for potential future reference. To implement this method effectively, it is necessary to save the robot coordinates for each image.

The pupil scan and the field reconstruction methods are proven to work with the POC setup in the laboratory environment. The next phase involves validating these methods using the WG-IQ prototype and optimizing the complete process. This field reconstruction is a possible solution for the referencing as it allows the camera and projector to remain adjacent throughout the measurement sequence. It has the potential to substantially reduce system complexity and overall costs.

6. CONCLUSION

Referencing is a critical component of high-accuracy optical measurement systems, given its profound impact on the reliability of the tester. In this thesis, an innovative and new way to achieve referencing of the waveguide measurement system was explored, effectively removing the need for pupil matching. Referencing has previously caused numerous challenges for optical and mechanical designers, as every moving part introduced inaccuracies into the system. It also adds a lot of cost for measurement systems as accurate and complex robots are required.

The presented field reconstruction method shows a groundbreaking solution to remove additional degrees of freedom from the system by removing the need for pupil matching. This results into a reduction in both cost and complexity. The motivation for such a system is the future of AR waveguide testing when manufacturers start to mass-produce waveguides and need a fast and reliable measurement system with as little complexity as possible.

In this thesis, a method was shown to overcome the adverse effects of pupil mismatch. The Nautilus experiment demonstrates that the usage of dual mirrors and mismatched pupils does not significantly decrease the MTF performance of the system. However, the Nautilus experiment alone does not conclusively establish the feasibility of referencing, as it is limited by a small FOV. Based on the pupil scanning experiment one can conclude that the field reconstruction method can be used. By comparing the reference image at pupil match and field reconstructed reference image it can be noticed that the information of referencing doesn't decrease. This result is backed by the MTF analysis.

The thesis presented two distinct algorithms for field reconstruction, both of which were successfully validated to be effective. Both of the algorithms give similar results and both have their pros and cons. Nonetheless, it is important to optimize the algorithm carefully. Since the mirrors introduce image rotation, the reference image must be accurately rotated and shifted back to its original orientation and location before utilizing the information from the reference image. This step is crucial to ensure the reliability and accuracy of the field reconstruction method in practical applications.

This thesis provides a robust foundation for future designs of the WG-IQ manufactured by OptoFidelity. The experimental findings presented in this thesis serve as a valuable

reference for evaluating the feasibility of employing field reconstruction in forthcoming measurement systems. By integrating this method as a replacement for pupil-matching referencing, it is anticipated that it will significantly reduce the overall complexity and cost of the WG-IQ system. Additionally, the outcomes of these experiments can be adapted to other applications where pupil matching presents challenges.

REFERENCES

[1] *Light. physics*. May 15, 2023. URL: https://www.britannica.com/science/light/Early-particle-and-wave-theories (visited on 06/14/2023).

[2] *Visible Light. What is the visible light spectrum?* July 22, 2023. URL: https://science.nasa.gov/ems/09_visiblelight (visited on 07/22/2023).

[3] *Human eye. anatomy*. Apr. 19, 2023. URL: https://www.britannica.com/science/human-eye/The-retina (visited on 06/14/2023).

[4] *How Does a Camera Work?* Jan. 10, 2023. URL: https://expertphotography.com/how-does-a-camera-work/ (visited on 06/14/2023).

[5] Romano Antonio. *Geometric Optics*. Birkhäuser Boston, MA, 2009. ISBN: 978-0-8176-4872-5. DOI: 10.1007/978-0-8176-4872-5. URL: https://link-springer-com.libproxy.tuni.fi/book/10.1007/978-0-8176-4872-5.

[6] C. Hoffman and R. Driggers. *Encyclopedia of Optical and Photonic Engineering (Print) - Five Volume Set*. CRC Press, 2015. ISBN: 9781351247177. URL: https://books.google.fi/books?id=prMIEAAAQBAJ.

[7] A.E. Conrady. *Applied Optics and Optical Design, Part Two*. Dover Books on Physics. Dover Publications, 2014. ISBN: 9780486162621. URL: https://books.google.fi/books?id=-kJ-GDnmxsAC.

[8] Matt Young. “Imaging Optics”. In: *Encyclopedia of Physical Science and Technology (Third Edition)*. Ed. by Robert A. Meyers. Third Edition. New York: Academic Press, 2003, pp. 645–660. ISBN: 978-0-12-227410-7. DOI: https://doi.org/10.1016/B0-12-227410-5/00328-8. URL: https://www.sciencedirect.com/science/article/pii/B0122274105003288.

[9] *Marginal and Chief Rays*. URL: https://spie.org/publications/pm92_161_marginal_chief_rays?SSO=1 (visited on 07/03/2023).

[10] *Ray (optics)*. Mar. 14, 2023. URL: https://en.wikipedia.org/wiki/Ray_(optics) (visited on 06/14/2023).

[11] Michael J. Kidger. *Fundamental Optical Design*. SPIE, 2001. 314 pp.

[12] Virendra N. Mahajan. SPIE, 1998. ISBN: 978-0-8194-2515-7. URL: https://app.knovel.com/hotlink/toc/id:kpOIAPIRG9/optical-imaging-aberrations-2/optical-imaging-aberrations-2.

[13] *Field of View*. URL: https://spie.org/publications/fg01_p27_field_of_view?SSO=1 (visited on 07/03/2023).

[14] *Understanding AR 1: Field of View*. Jan. 1, 2023. URL: https://waveoptics.ar/blog/understanding-ar-1-field-of-view/ (visited on 07/03/2023).

[15] A. E. Conrady. Dover Publications, 1985; 1988. ISBN: 978-0-486-67007-2; 978-0-486-67008-9. URL: https://app.knovel.com/hotlink/toc/id:kpAOODPOT3/applied-optics-optical/applied-optics-optical.

[16] *What is FOV, Exit Pupil, and Eye Relief?* Sept. 19, 2023. URL: https://www.displaymodule.com/blogs/knowledge/what-is-field-of-view-exit-pupil-eye-relief (visited on 07/31/2023).

[17] *Eye relief*. June 11, 2023. URL: https://en.wikipedia.org/wiki/Eye_relief (visited on 07/03/2023).

[18] Kress Bernard C. *Optical Architectures for Augmented-, Virtual-, and Mixed-Reality Headsets*. SPIE, 2020. 253 pp.

[19] *Constructing a Flat Field for Scientific Astronomical Imaging*. 2014. URL: https://digitalcommons.usu.edu/phys_capstoneproject/10/?utm_source=digitalcommons.usu.edu%2Fphys_capstoneproject%2F10&utm_medium=PDF&utm_campaign=PDFCoverPages (visited on 07/31/2023).

[20] *Flat Field Correction*. Dec. 15, 2011. URL: https://web.archive.org/web/20130407013841/http://www.princetoninstruments.com/cms/index.php/ccd-primer/152-flat-field-correction (visited on 07/31/2023).

[21] Sasián José. *Introduction to Aberrations in Optical Imaging Systems.* Cambridge University Press, 2012. ISBN: 9781107006331. URL: http://libproxy.tuni.fi/login?url=https://search.ebscohost.com/login.aspx?direct=true&AuthType=cookie,ip,uid&db=e000xww&AN=508282&site=ehost-live&scope=site.

[22] *Optical Aberrations*. URL: https://www.eckop.com/resources/optics/aberrations/ (visited on 07/03/2023).

[23] Sebastián Mirasol-Menacho et al. “Development of a HMD for Virtual Acoustics. Application in a World Heritage (UNESCO) Building from the Valencian Civil Gothic”. In: (June 2016), pp. 241–250. DOI: 10.1007/978-3-319-40651-0_19.

[24] DANIEL J. SCHROEDER. “Chapter 5 - Fermat’s Principle and Aberrations”. In: *Astronomical Optics (Second Edition)*. Ed. by DANIEL J. SCHROEDER. Second Edition. San Diego: Academic Press, 2000, pp. 70–111. ISBN: 978-0-12-629810-9. DOI: https://doi.org/10.1016/B978-012629810-9/50006-2. URL: https://www.sciencedirect.com/science/article/pii/B9780126298109500062.

[25] *Sony’s curved sensors may allow for simpler lenses and better images*. June 18, 2014. URL: https://www.dpreview.com/articles/2279255612/sony-s-curved-sensors-may-allow-for-simpler-lenses-and-better-images (visited on 07/31/2023).

[26] Ana Valerga et al. “Photogrammetry as an Engineering Design Tool”. In: June 2020. ISBN: 978-1-83968-212-4. DOI: 10.5772/intechopen.92998.

[27] Forrest L. Anderson. “Huygens’ Principle geometric derivation and elimination of the wake and backward wave”. In: *Scientific Reports* 11 (2021). ISSN: 2045-2322. DOI: 10.1038/s41598-021-99049-7. URL: https://doi.org/10.1038/s41598-021-99049-7.

[28] John Appel. *"Diffraction." The Gale Encyclopedia of Science*. Gale eBooks, 2021. ISBN: 978-0-02-867717-0. URL: https://link-gale-com.libproxy.tuni.fi/apps/doc/CX8124400761/GVRL?u=tampere&sid=bookmark-GVRL&xid=df5351e4.

[29] William S. C. Chang. Cambridge University Press, 2015. ISBN: 978-1-107-07490-3. URL: https://app.knovel.com/hotlink/toc/id:kpPOEDMA01/principles-optics-engineers/principles-optics-engineers.

[30] Gregory Hollows and Nicholas James. *The Airy Disk and Diffraction Limit*. URL: https://www.edmundoptics.eu/knowledge-center/application-notes/imaging/limitations-on-resolution-and-contrast-the-airy-disk/ (visited on 07/04/2023).

[31] *What is the Modulation Trasnfer Function?* URL: https://www.olympus-lifescience.com/en/resources/white-papers/what-is-the-modulation-transfer-function/ (visited on 06/30/2023).

[32] *Contrast*. Jan. 14, 2023. URL: https://www.edmundoptics.eu/knowledge-center/application-notes/imaging/contrast/ (visited on 06/30/2023).

[33] *Contrast (vision)*. June 24, 2023. URL: https://en.wikipedia.org/wiki/Contrast_(vision) (visited on 06/30/2023).

[34] Philip Yip. “Nanometrology using Time-Resolved Fluorescence”. PhD thesis. Apr. 2016. DOI: 10.13140/RG.2.1.4045.2084.

[35] Ting-Wei Shen et al. “Improving Image Quality Assessment Based on the Combination of the Power Spectrum of Fingerprint Images and Prewitt Filter”. In: *Applied Sciences* 12.7 (2022). DOI: 10.3390/app12073320. URL: https://www.mdpi.com/2076-3417/12/7/3320.

[36] *Introduction to Modulation Transfer Function*. URL: https://www.edmundoptics.com/knowledge-center/application-notes/optics/introduction-to-modulation-transfer-function/ (visited on 07/04/2023).

[37] *Forschungsprojekt PHABULOuS: Aufbau von Kompetenzen und einer Anlaufstelle*. URL: https://www.swissmem.ch/de/aktuelles/detailansicht/forschungsprojekt-phabulous-aufbau-von-kompetenzen-und-einer-anlaufstelle.html (visited on 07/05/2023).

[38] J. Xiong et al. “Augmented reality and virtual reality displays: emerging technologies and future perspectives”. In: *Light: Science & Applications* 10 (2021). DOI: 10.1038/s41377-021-00658-8. URL: https://www.nature.com/articles/s41377-021-00658-8.

[39] Artem Solomashenko et al. “Image Quality for Near-Eye Display Based on Holographic Waveguides”. In: *Applied Sciences* 12.21 (2022). ISSN: 2076-3417. DOI: 10.3390/app122111136. URL: https://www.mdpi.com/2076-3417/12/21/11136.

[40] Ying Kuang, Juan Liu, and Xueliang Shi. “Effect of surface roughness of optical waveguide on imaging quality and a formula of RSE tolerance and incident angle”. In: *Opt. Express* 28.2 (Jan. 2020), pp. 1103–1113. DOI: 10.1364/OE.382804. URL: https://opg.optica.org/oe/abstract.cfm?URI=oe-28-2-1103.

[41] Bernard Kress and Thad Starner. “A review of head-mounted displays (HMD) technologies and applications for consumer electronics”. In: 8720 (2013). Ed. by Alex A. Kazemi, Bernard C. Kress, and Simon Thibault, 87200A. DOI: 10.1117/12.2015654. URL: https://doi.org/10.1117/12.2015654.

[42] *About HoloLens 2*. Mar. 13, 2023. URL: https://learn.microsoft.com/en-us/hololens/hololens2-hardware (visited on 07/06/2023).

[43] *Magic Leap 2 at SPIE AR/VR/MR 2022*. Jan. 31, 2022. URL: https://kguttag.com/2022/01/31/magic-leap-2-at-spie-ar-vr-mr-2022/ (visited on 07/06/2023).

[44] *Ride the Wave: Augmented Reality Devices Rely on Waveguides*. Jan. 10, 2022. URL: https://www.radiantvisionsystems.com/blog/ride-wave-augmented-reality-devices-rely-waveguides (visited on 07/06/2023).

[45] *International Electrotechnical Commission Standards*. URL: https://webstore.iec.ch/home (visited on 07/08/2023).

[46] *American National Standards Institute Standards*. URL: https://www.ansi.org/ (visited on 07/08/2023).

[47] *ICDM Standards*. URL: https://www.sid.org/ (visited on 07/08/2023).

[48] *ISO Standards*. URL: https://www.iso.org/standards.html (visited on 07/08/2023).

[49] International Electrotechnical Commission. *International Standard, Eyewear display-Part 20-10:Fundamental measurement methods - Optical properties*. 2019.

[50] Andriy Pavlovych and Wolfgang Stuerzlinger. “A high-dynamic range projection system”. In: *Proc SPIE* (Sept. 2005), pp. 636–643. DOI: 10.1117/12.629117.

[51] *The Myth of High Contrast. What is those contrast terms mean? Is high contrast good?* Mar. 2, 2020. URL: https://www.benq.com/en-us/knowledge-center/knowledge/the-myth-of-high-contrast.html (visited on 07/07/2023).

[52] International Committee for Display Metrology (ICDM). *Information Display Measurements standard*. 2023. DOI: 10.55410/dnaw9661.

[53] Kenichiro Masaoka et al. “Modified slanted-edge method and multidirectional modulation transfer function estimation”. In: *Opt. Express* 22.5 (Mar. 2014), pp. 6040–6046. DOI: 10.1364/OE.22.006040. URL: https://opg.optica.org/oe/abstract.cfm?URI=oe-22-5-6040.

[54] *OptoFidelity WG-IQ. Fully automated waveguide image quality measurement system*. 2023. URL: https://www.optofidelity.com/products/wg-iq (visited on 07/08/2023).

[55] Alessandro Artusi et al. “High Dynamic Range Imaging Technology [Lecture Notes]”. In: *IEEE Signal Processing Magazine* 34 (Sept. 2017), pp. 165–172. DOI: 10.1109/MSP.2017.2716957.